Microneedle-based drug delivery systems: Microfabrication, drug delivery, and safety

Donnelly, R. F., Raj Singh, T. R., & Woolfson, A. D. (2010). Microneedle-based drug delivery systems: Microfabrication, drug delivery, and safety. *Drug Delivery*, *17*(4), 187-207. https://doi.org/10.3109/10717541003667798

Published in:
Drug Delivery

Document Version:
Peer reviewed version

Queen's University Belfast - Research Portal:
Link to publication record in Queen's University Belfast Research Portal

Published in final edited form as:
Drug Deliv. 2010 May ; 17(4): 187–207. doi:10.3109/10717541003667798.

Microneedle-based drug delivery systems: Microfabrication, drug delivery, and safety

Ryan F. Donnelly, **Thakur Raghu Raj Singh**, and **A. David Woolfson**
School of Pharmacy, Queen's University Belfast, Medical Biology Centre, 97 Lisburn Road, Belfast BT9 7BL, UK

Abstract

Many promising therapeutic agents are limited by their inability to reach the systemic circulation, due to the excellent barrier properties of biological membranes, such as the *stratum corneum* (*SC*) of the skin or the sclera/cornea of the eye and others. The outermost layer of the skin, the *SC*, is the principal barrier to topically-applied medications. The intact *SC* thus provides the main barrier to exogenous substances, including drugs. Only drugs with very specific physicochemical properties (molecular weight < 500 Da, adequate lipophilicity, and low melting point) can be successfully administered transdermally. Transdermal delivery of hydrophilic drugs and macromolecular agents of interest, including peptides, DNA, and small interfering RNA is problematic. Therefore, facilitation of drug penetration through the *SC* may involve by-pass or reversible disruption of *SC* molecular architecture. Microneedles (MNs), when used to puncture skin, will by-pass the *SC* and create transient aqueous transport pathways of micron dimensions and enhance the transdermal permeability. These micropores are orders of magnitude larger than molecular dimensions, and, therefore, should readily permit the transport of hydrophilic macromolecules. Various strategies have been employed by many research groups and pharmaceutical companies worldwide, for the fabrication of MNs. This review details various types of MNs, fabrication methods and, importantly, investigations of clinical safety of MN.

Keywords

MEMS; silicon; metal; polymer; stratum corneum

Introduction

Microneedles (MNs) consist of a plurality of micro-projections, generally ranging from 25–2000 μm in height, of different shapes, which are attached to a base support. Application of MN arrays to biological membranes can create transport pathways of micron dimensions (Kaushik et al., 2001). Once created, these micropores or pathways are orders of magnitude larger than molecular dimensions and, therefore, should readily-permit transport of macromolecules, as well as possibly supramolecular complexes and microparticles (Prausnitz, 2004). In addition, MNs could also be used for sampling body fluids, such as for measuring the blood glucose levels in diabetic therapy. ALZA corporation appear to be the

Address for Correspondence: Dr Ryan F. Donnelly, Lecturer in Pharmaceutics, School of Pharmacy, Queens University Belfast, Medical Biology Centre, 97 Lisburn Road, Belfast BT9 7BL, UK. Tel: +44 (0) 28 90 972 251. Fax: +44 (0) 28 90 247 794. r.donnelly@qub.ac.uk.

Declarationof interest
The authors report no conflicts of interest. The authors alone are responsible for the content and writing of the paper.

first to conceive MNs, described in a 1976 patent (Gerstel & Place, 1976). However, it was not possible to make such microstructured devices until the 1990s, with the advent of high precision microelectronics industrial tools. The first paper to demonstrate MNs for transdermal delivery was not published until 1998 (Henry et al., 1998).

MNs have been shown to penetrate the skin, across the *stratum corneum* (*SC*), and into the viable epidermis (*VE*), avoiding contact with nerve fibers and blood vessels that reside primarily in the dermal layer. Therefore, the principal benefit of using MNs is the promise of pain-free delivery of both small and large molecular weight active pharmaceutical ingredients (APIs) (Kaushik et al., 2001). Extensive research has been reported in the literature concerning the manufacture of different types of MNs using different techniques. Importantly, microfabrication technology, and enhancement in the delivery of drugs and biomolecules of a wide variety of physicochemical properties, has been demonstrated in in vitro, ex vivo, and in vivo experiments. This review summarizes the production of MN devices used for the creation of micropores in biological membranes, such as skin, mucosal tissue, and sclera, to enhance the permeability of therapeutic agents. In addition, it also addresses the safety of MNs presently in either pre-clinical or clinical studies.

Methods of fabricating microneedles

The first MN devices were fabricated from silicon (Hashmi et al., 1995; Henry et al., 1998), but many other materials have also been used in MN fabrication, such as stainless steel (Verbaan et al., 2007), dextrin (Ito et al., 2006a; b), glass (Wang et al., 2000), ceramic (Ovsianikov et al., 2007), maltose (Miyano et al., 2005; Kolli & Banga, 2008), galactose (Donnelly et al., 2009a), and various polymers (McAllister et al., 2003; Park et al., 2005; 2006; Perennes et al., 2006). Over the past few years, investigators have used a multiplicity of methods in the manufacture of a wide variety of MNs, such as conventional microelectronics fabrication technologies, including chemical isotropic etching, injection moulding, reactive ion etching, surface/bulk micromachining, polysilicon micromoulding, lithography-electroforming-replication, and laser drilling (Trichur et al., 2002; Yang & Zahn, 2004; Davis et al., 2005; Moon et al., 2005; Park et al., 2005; Stoeber & Liepmann, 2005). Moreover, MNs have been fabricated with a wide range of designs (different sizes and shapes) and different types (solid, hollow, sharp, or flat). The two basic designs are: in-plane (Figure 1a) and out-of-plane (Figure 1b). However, a combination of both in-plane and out-of-plane (Figure 1c) designs has also been reported. In in-plane designs, the MNs are parallel to the fabrication surface; whereas in out-of-plane designs, the MNs are perpendicular to the fabrication surface (Sivamani et al., 2007).

Manufacturing methods for silicon microneedles by microfabrication

Microfabrication technology, i.e. micro-machining or micro-electromechanical systems (MEMS), traditionally applied to produce microprocessors, is currently applied in the manufacture of micron-scale devices, such as micropumps, microreactors, accelerometers, and micromirrors (Jing et al., 2006). Exploitation of these MEMS techniques has led to potential applications in biomedical fields (called BioMEMS), such as in drug delivery, DNA sequencing devices, biosensors, and chemical analysis systems (Katsuma & Tsujimoto, 2001; Lindner, 2001; Leoni & Desai, 2004). MEMS technology can be efficiently applied in the fabrication of MN arrays (Tao & Desai, 2003;). Although these tools offer the potential for mass production of MNs, production is often highly specialized and includes complex multi-step processes (Zafar et al., 2004; Ziaie et al., 2004).

MEMS technology utilizes a number of tools and methodologies to create small three-dimensional (3D) structures, with dimensions ranging from sub-centimeter to sub-micrometer. MEMS technology is significantly adapted from that of integrated circuit (IC)

technology. In a MEMS process, before the actual device is generated, a series of sequential operations are necessary. The three basic techniques in MEMS technology are to apply a patterned mask on top of a film by photolithograpic imaging, the deposition of thin films of material on a substrate and etching the films selectively to the mask (Madou, 1997; Banks, 2006).

Basics of silicon microfabrication

Lithography: Both in microelectronics and micromachining, fabrication starts with lithography (lithos 'stone' and gráphein 'to write'); the technique used to transfer the master pattern onto the surface of a substrate (e.g. silicon wafer), previously coated with a photosensitive material, by selective exposure to a radiation source (e.g. UV light). The most widely used type of lithography is photolithography (Le Barny, 1987; Moreau, 1988; Metz et al., 1992; Madou 1997; Banks, 2006).

Thin-film deposition on substrate: One of the basic steps in the MEMS process is the deposition of a thin film on the substrate surface (e.g. silicon wafer). These films can then be patterned using photolithographic techniques and suitable etching techniques. Common materials include silicon dioxide (oxide) and silicon nitride (nitride) (Banks, 2006). Thin-film deposition on the substrate can be also be achieved by using a wide range of materials, including noble metals such as gold (Madou, 1997).

In general, in physical vapor deposition (PVD) based techniques, the raw materials (solid, liquid, or vapor) are released from the source (material to be coated) and deposited on the substrate surface. For instance, in thermal evaporation, the silicon wafer is placed inside a vacuum chamber and the source (e.g. aluminium) is heated by electron-beam or radio-frequency. The heating causes the source to boil and the vapors are then condensed onto the substrate surface to form a film. In the sputtering technique, the substrate and source is placed in a chamber containing inert gas (e.g. argon or Xe) at low pressure. Using a power source, the gas plasma is ionized which then accelerates the ions, promoting them to impinge on the substrate surface (Madou, 1997).

In chemical vapor deposition (CVD), thin-films are produced by a chemical reaction between the hot substrate and inert-carrier gases in the chamber. The CVD method is versatile and works at low or atmospheric pressure at relatively low temperatures. The two most common CVD technologies in MEMS are the LPCVD and PECVD. The LPCVD allows coating of large numbers of wafers without detrimental effects on film uniformity at higher temperatures (> 600°C). On the other hand, PECVD operates at low temperatures and films grow at a faster rate (Adams, 1988; Jensen, 1989).

Finally, the choice of a specific deposition process is dependent upon a variety of considerations, such as substrate structure, source (e.g. chemistry, purity, or thickness), apparatus, operating temperature, rate of deposition, and total production time. After deposition, the thin-film can be locally etched using lithographic or etching processes to create the final device (Banks, 2006).

Etching: Following lithography, and to create the final functional form of MEMS structure on a substrate, it is necessary to etch the thin-films previously deposited and/or the substrate itself. In general, there are two classes of etching processes: wet etching and dry etching.

- *Wet etching*: In this process, the material is removed by immersing the wafer in a liquid bath containing a chemical etchant. The two main wet etching techniques are isotropic and anisotropic etching. Isotropic etchants attack the material, such as oxide, nitride, aluminium, polysilicon, gold, and silicon, at the same rate and in all

directions. They remove material horizontally under the etch mask (under-cutting). In contrast, anisotropic etchants attack the material (silicon wafer) at different rates in different directions, to produce more controlled shapes. The crystal planes in silicon limit anisotropic wet etching (Kern, 1978; Clark & Edell, 1987; Shikida et al., 2000; Banks, 2006).

- *Dry etching*: This form of etching is carried out at low pressure in the presence of inert or reactive gases. Dry etching is categorized into two main types: reactive ion etching (RIE), which involves chemical processes, and ion-beam milling, which involves purely physical processes (Banks, 2006).

Fabrication of silicon microneedles—For decades, puncturing of the human skin with hollow hypodermic needles (HNs) has been the universally-accepted, invasive, medical procedure for injecting drugs or collecting biological samples (McAllister et al., 2000). However, HNs-mediated injections are still painful and also remain a common cause of medical device-related infections (Arduino et al., 1997; Prausnitz, 2004). In addition, one must dispose of HNs after use in special bins which further requires expensive treatments of disposal. However, the design of HNs, a two-directional flow of fluids for both drug delivery and biological fluid extraction, has guided researchers to design micron-sized needles, called hollow MNs (HMNs). HMNs, resembling the sharp HN, are intended to be used as minimally invasive means of overcoming the outermost barrier of the skin, the *SC*, for both drug delivery and/or biological fluid sampling (Mukerjee et al., 2004). Microfabrication techniques have been effectively used to manufacture both solid and hollow MNs.

In the first published study, solid silicon MNs arrays were fabricated by a RIE process, with a chromium mask, which is a dry-etch process (Henry et al., 1998). Similarly, different research groups have used either wet- or dry-etching technique for fabricating solid MNs (SMNs) of varying shapes, heights, and densities from silicon. In SMNs fabrication using a wet-etch process a standard silicon wafer (P-type) is deposited with an oxide layer (300 Å) and a layer of nitride (1000 Å) using a standard LPCVD process. The double layer was patterned with a plasma etch and 280 μm high MN arrays (with aspect ratio 3:2) were fabricated using 29% KOH v/v at 79°C at an etch rate of 1.12 (± 0.02) μm/min (Wilke et al., 2005). Apart from wet etching, Wilke et al. (2005) have also demonstrated both solid and hollow MN fabricated by a dry etching technique. Using a standard wafer of 525 μm thickness, conical-shaped solid MNs with an aspect ratio of 4.5:1 (height:base diameter) were fabricated by a modified RIE process. A typically undercut etch rate to vertical etch (using SF_6/O_2) was used alternately with the BOSCH-DIRE process. For hollow MNs, an additional etching, from the backside of the silicon wafer, was performed using DIRE.

Paik et al. (2004) fabricated in-plane single-crystal-silicon MN arrays by a dry etching technique consisting of a microchannel (Figure 2a). The MN shafts, 2 mm in length, 100 μm wide, and of 100 μm thickness, were strong enough to endure a 0.248 mN of out-of-plane bending moment and 6.28 N of in-plane buckling load. This MN array, when integrated with a PDMS microfluid chip, was found to efficiently deliver model solutes, namely Rhodamine B dye and black ink, in in vitro (agarose gel) and ex vivo (chicken breast) models through the microchannel (Figure 2a). Roxhed et al. (2008a) proposed a novel concept of sharp hollow silicon MN tips with side-openings. Furthermore, the HMNs tips were sealed with thin leak-tight membranes to provide a closed-package system, which prevents drug degradation, evaporation on leaking-out and damage due to handling, thus improving the shelf-life of HMNs-based patch devices. The MN were etched on 600 μm thick, 100 mm, monocrystalline silicon wafers using a two-mask process, an anisotropic DRIE etch through the BOSCH process, and an isotropic (unbiased) SF_6 plasma etching. The needle bore was

first etched from the backside of the silicon wafer, after which needle geometry was shaped from the front side by mixed isotropic and anisotropic etching. An intersection between the two-directional etchings resulted in a side-opening of needles. The two designs of MN created were a 310 μm long cross-shaped MN (Figure 2bi) and 400 μm long circular-shaped MNs (Figure 2bii). The side-opening, which was previously coated with an adherent layer of 20 nm thick chromium, was sealed with a layer of gold coating of three different thicknesses (150, 300, and 450 nm). Three different approaches to open the seals were studied: burst opening, electrochemical opening, and opening upon insertion into the skin.

All three methods were found efficient in opening the side-bores. However, the biocompatibility of the residual coating material left in the skin was not demonstrated. Furthermore, Roxhed et al. (2008b) integrated the above-mentioned 400 μm long circular-shaped HMNs with a low-cost, electrically-controlled liquid dispensing unit to form a complete patch-like drug delivery system. The dispenser consisted of three distinct layers; a 500 μm thick printed circuit board (PCB) heater layer, a 500 μm thick expandable layer (a mixture of silicone elastomers), and a liquid reservoir (total volume of 12 μL) (Figure 2c). This integrated HMN device demonstrated successful delivery of insulin in diabetic rats, where active infusion at 2 μl/h showed consistent control over blood glucose levels when compared to passive (unactuated) delivery.

Rodriguez et al. (2005) fabricated hollow silicon dioxide MNs on the backside of an *n*-type Si wafer by using an electrochemical etching process. MNs with different geometries and lengths ranging from 30–140 μm, with wall thickness from 70–110 nm and pore diameters between 2–5 μm were etched on the macroporous silicon (Figure 2d). To control the fluidic properties of the micro-structures, the MNs were glued to a tube which, in turn, was attached to a syringe. This, in theory, should allow a controlled delivery of the loaded dose with high precision. Bin et al. (2006) presented a piezoelectric (PZT) micropump integrated with an array of HMNs. The HMNs (Figure 2e) were fabricated on a flexible silicon substrate by inductively coupled plasma (ICP) and anisotropic wet-etching techniques (200 μm height, 30 μm internal, and 90 μm outer diameters). The PZT pump is connected to a flexible MN array to create a prototype device, in which the total size of the packaged micropump is claimed to be smaller than any other packages of insulin pump, which can perform precise fluid sampling, programmable drug delivery, remote operation, and autonomy.

Ramasubramanian et al. (2008) showed an interesting approach towards the design of HMNs. The authors considered the naturally-existing mosquito fascicle, which painlessly draws blood from the human skin surface. The anatomical details and the dynamics of mosquito fascicle penetration were studied by scanning electron microscopy (SEM) and high-speed video imaging, respectively (Figure 2f). Mathematical models were used to determine the role of the lateral support of the fascicle (labium) and non-conservative force application. Results showed that the lateral support of the labium is critical and helps the mosquito to penetrate the skin. In general, the fascicle is typically 1.8 mm long and has an internal radius of 11 μm, with a blood withdrawal volume of 4.2 ml taking ~ 141 s. Thus, careful attention towards the anatomical dimensions and dynamics of mosquito bites may help the design of novel MNs.

Manufacturing methods of metal and other types of microneedles

Although silicon is attractive, as a common microeletronics substrate with extensive processing experience for more than 30 years, it is relatively expensive and requires clean room processing (Banga, 2009). In contrast, metal and glass MNs have been found to be equally effective in skin penetration and can be produced at relatively much lower cost than silicon MNs. Various metals, such as stainless-steel, titanium, palladium, palladium-cobalt alloys, and nickel has been used as structural materials for MN fabrication (Chandrasekaran

& Frazier, 2003; Chandrasekaran et al., 2003; Verbaan et al., 2008). A number of approaches have been investigated for fabricating metal MNs, such as electroplating (palladium), photochemical etching (titanium), and laser cutting (stainless-steel). Metals such as stainless-steel (e.g. hypodermic needles) have been in medical use for decades. Essentially, the use of such materials will effectively reduce the regulatory path of approval, compared with that required for non-approved material, such as silicon (Mikstza et al., 2006). In addition, like silicon MNs, metals can be routinely fabricated into both solid and hollow MNs.

The simplest form of solid metal MNs were made by assembling stainless steel wires of 200 μm diameter and 300 μm height (4 × 4 array), where the tips were cut tangentially to obtain sharp tips. These assembled MNs were used to pierce dermatomed human skin either manually or using an electrically-driven applicator. It was observed that the flux of cascade blue through the MN treated skin was 70 ± 21 and 44 ± 17 pmol/cm^2/h, for MNs accelerated at a velocity of 3 m/s and 1 m/s, respectively, using the electric applicator, and 6 ± 3 pmol/cm^2/h using a manual applicator (Verbaan et al., 2008).

Badran et al. (2009) utilized a novel MN device called a Dermaroller®, with different stainless steel needle lengths (150, 500, and 1500 μm) protruding out from a cylindrical assembly containing 24 circular arrays of eight needles each (192 needles in total). Martanto et al. (2004) fabricated arrays of MN shafts from stainless steel sheets (75 μm thick) using an infrared laser, where the shape and orientation of the arrays were drafted by AutoCAD software. The laser was operated at 1000 Hz at an energy density of 20 J/cm^2, taking a total of 4 min to cut an array. Each needle was manually bent at 90° to create an out-of-plane MN array from the sheet, which was electropolished (6:3:1, glycerine:phosphoric acid:water). Wu et al. (2007) assembled acupuncture needles on a silicon sheet (1.0 × 20 × 20 mm). Each needle tapered over a 400 μm length with a tip angle of 28° angle, with a base diameter of 200 μm.

Conventional hypodermic needles (HNs) have also been used to produce hollow MNs (HMNs). The smallest used HNs were manually assembled to form an array of MNs. Currently, the smallest used HNs are 30 and 31 gauge (G) attached to syringes and pen injectors (for insulin delivery) has outer diameters of 305 and 254 μm, respectively (Trimmer et al., 1995). Verbaan et al. (2007) used commercially available 30G HNs and assembled them in 4 × 4 arrays, supported by a polyetheretherketone mould, with needle heights adjusted to 300, 550, 700, and 900 μm. These 30 G stainless steel HNs were chosen due to their low cost and robustness compared to silicon, which is brittle and not biocompatible (Runyan & Bean, 1990; Braybrook, 1997). A similar design, employing 1 mm long HMNs, was proposed by using 34G stainless steel HNs fitted to a 1 ml syringe for vaccine delivery in rat models (Dean et al., 2005; Jason et al., 2007). However, in these applications, the role of HMNs was similar to that of SMNs, where drug is applied after removal of MNs. In such a case, the role of the hollow bores in the MNs becomes irrelevant. Furthermore, these types of HMNs are limited in terms of designs; the only feasible modification is the needle height. Alternatively, Martanto et al. (2006a) fabricated a single hollow glass MN by pulling fire-polished glass pipettes using a micropipette puller and the resulting blunt-tip MN was beveled (at an angle of 35–38°) and cleaned in a series of solutions. These cleaned MN were attached to a 250 μL or 1 ml glass syringe (containing 1 × 10^{-3} M sulfurhodamine B solution) and were investigated for infusion flow rates into human cadaver skin.

While both silicon and metal MNs have been widely employed in experiments carried out by research groups and industry worldwide, to date their real clinical usefulness is still in doubt. Neither material type is biodegradable, leading to questions about what happens to

broken microneedles left behind in the skin (Prausnitz, 2004). Silicon requires clean room processing and, unlike titanium, for example, is not an FDA-approved biomaterial (Runyan & Bean, 1990). Wet etch processing of silicon is limited in terms of the needle height and inter-spacing achievable, and HMNs can become blocked, thus reducing greatly drug delivery. If HMNs are broken during application, a significant leakage or misdosage may occur (Down & Harvey, 2003). While many metals are undoubtedly cheaper and stronger than silicon there are concerns about the immuno-inflammatory response of soft tissue around stainless steel and titanium implants (Braybrook, 1997).

Manufacturing methods for polymeric mcroneedles

Polymeric MNs are now gaining importance, due to a variety of properties, such as biocompatibility, biodegradability, strength, toughness, and optical clarity (Aoyagi et al., 2007; Jeong et al., 2008). In addition, polymeric MN fabrication and reproducibility is considerably more cost-effective when compared to that of typical MEMS processes. To accurately produce the micro-scale dimensions of polymer MNs, a variety of mould-based techniques, such as casting (Perennes et al., 2006; Lippmann et al., 2007), hot embossing (Han et al., 2009), injection molding (Sammoura et al., 2007), and investment molding (Lippmann et al., 2007) have been investigated. Polymeric materials which have been efficiently fabricated into MNs include; poly (methylmetha-acrylate) (PMMA), poly-L-lactic acid (PLA), poly-glycolic acid (PGA), and poly-lactic-co-glycolic acid (PLGA), cyclic-olefin copolymer, poly (vinyl pyrrolidone), and sodium carboxymethyl cellulose (Moon & Lee, 2005; Park et al., 2005; Perennes et al., 2006; Aoyagi et al., 2007; Han et al., 2007; Lippmann et al., 2007; Ovsianikov et al., 2007; Sammoura et al., 2007; Sullivan et al., 2008). Sugars have also been used to fabricate the MNs, such as galactose, maltose, and dextrin (Miyano et al., 2005; Kolli & Banga, 2008; Donnelly et al., 2009a).

Park et al. (2005) fabricated three different types of master structures, namely beveled-tip, chisel-tip, and tapered-cone to form polydimethylsiloxane (PDMS) molds from which PLA, PGA, and PLGA biodegradable MNs were formed. All three MN designs had failure forces much greater than the insertion forces. Polymeric MN puncture of human cadaver epidermis caused an increase in calcein and BSA permeability by almost 2 (20-MN array) or 3 (100-MN array) orders of magnitude. In addition, Park et al. (2007) also fabricated MN master structures using microlenses etched onto a glass substrate that focused light through SU-8 negative epoxy resists, producing sharply-tapered structures. Using these master structures, PDMS micromolds were produced which, in turn, produced PLA, PGA, and PLGA MNs, which were assessed mechanically. In vivo MN insertion force in human skin increased with increase in tip area (0.037–0.6 N per needle for MNs with tip diameters of 20–80 μm) and MN failure force decreased with increasing MN length (0.22 N for 700 μm to 0.1 N for 1500 μm). It was reported that the PDMS molds were reusable for producing polymer MNs for at least 100 times.

Moon and Lee (2005) have developed out-of-plane HMN arrays of poly(methylmetha acrylate) (PMMA) using deep x-ray lithography (DXRL). Unlike the conventional LIGA process employing the DXRL fabrication techniques, the present method employed two successive exposures of DXRL, a vertical DXRL and an inclined DXRL, for simultaneous fabrication of long and tapered-shaped MNs. The process employed high-energy photons, i.e. DXR exposure to make high-aspect-ratio microstructures out of PMMA, a biocompatible material. The height of 3D-shaped triangular HMNs ranged from 750–1000 μm with a base diameter from 270–400 μm and bore diameter between 70–100 μm. The performance of the MNs was tested manually on two spots of human skin, the fingertip and back of the hand. Due to higher thickness and flexibility of finger tips, MNs (750 μm high) did not penetrate the dermis layer to extract blood samples. In contrast, blood samples were easily collected from skin on the back of the hand. However, this method did not present any

replication technique for the MN array. In contrast, Perennes et al. (2006) manufactured sharp beveled tip PMMA HMNs by the DXRL process and showed the replication technique of PMMA HMN arrays using soft polymeric molds of poly(vinyl alcohol) (PVA). A two-step DXRL application on 2.7 mm thick PMMA sheets produced saw-toothed hollow PMMA MN arrays, which were electroplated with a metal layer to ensure the rigidity of the device. These MN were then used as master templates. The master templates were then used to cast soft materials, such as PDMS or PVA, in the liquid state and peeled off once solidified to produce a mold, reproducing a 3D negative stamp of MN arrays. In the case of PVA molds, the casting liquid of PMMA was poured on top of the PVA mold and left for 3–4 h at room temperature for polymerization. The PVA/PMMA assembly was then immersed in water at 40°C for 2 h to dissolve the PVA, leaving behind the PMMA MN arrays. In contrast, PDMS did not create efficient molds, due to a lack of stiffness of polymerized PDMS, which led to the crawling of high aspect ratio pillars. Therefore, PDMS was replaced with the soluble PVA. Using a similar technique, Matteucci et al. (2009) created re-usable PVA masters for MN replication. Both hollow and solid PMMA MN arrays of different shapes and of height between 500–1100 μm were fabricated using PVA masters to replicate at least 10 PMMA MN arrays.

Lippmann et al. (2007) used investment molding, a combination of investment (sacrificial element) casting and injection molding, to create in-plane HMNs. A plastic polymer called Cyclic Olefin Copolymer (COC) was used for its balance of strength, ease of manufacturing, and its biocompatibility to produce hollow-type MNs. The hollow, in-plane, polymeric MNs were 280 μm in height, had a width at base of 130 μm, and a bore diameter of 35 μm. Similarly, Sammoura et al. (2007) fabricated in-plane, open-channel polymeric MN via microinjection molding techniques. The key components were the shank portion (4.7 mm) with an open-channel (cross-sectional area of 0.1 × 0.1 mm) and the base portion consisting of a reservoir. In this study Topas®COC, a copolymer based on cyclic olefins and ethylene, was used as the plastic material for making in-plane MN by injection molding. Upon application into beef liver, these MN were observed to draw 0.04 μL of liquid immediately from tissues.

Han et al. (2007) used a casting technique to design a prototype MN array, in which in-plane was transformed to out-of-plane biocompatible polycarbonate MN arrays. Firstly, the in-plane MNs were fabricated using inclined UV lithography and electroforming. The in-plane MNs were then aligned parallel to each other to form an out-of-plane MN array. For mass production, a negative mold of PDMS was fabricated by replicating the out-of-plane MN array. Finally, the biocompatible out-of-plane MNs were produced using a hot-embossing machine.

Aoyagi et al. (2007) created an interesting HMN design, in which they used a UV excimer laser to create hollow polymeric MNs. Briefly, the laser was applied to create long thin holes with a diameter of 10, 20, or 50 μm and of varying depths in the biodegradable polymeric material (i.e. PLA). The investigators also developed long PLA MNs, which were subjected to laser pulses to create holes (10 μm in diameter) within the central core of the MN. Blood collection through the HMNs was successfully demonstrated.

Unlike the conventional silicon, steel, or titanium micro-fabrication processes, Ovsianikov et al. (2007) illustrated a two-photon polymerization (2PP) technique to create in-plane and out-of-plane HMN arrays using a covalently bonded organic–inorganic material called Ormocer® (organically modified ceramic) as substrate. Briefly, in the 2PP method, a femtoseconds laser pulse (60 fs, 94 MHz, < 450 mW, 780 nm) from a titanium:sapphire laser was focused into a small focal volume within a photosensitive resin, where the laser pulse cleaved chemical bonds, and the desired structures were fabricated by moving the

laser focus in three-dimensions. Three different designs of HMNs were produced, with different bore sizes and positions. The HMNs fabrication time for a single MN was 2 min, with needle height of 800 μm and base diameter of 150–300 μm. Significantly, this is the only study conducted to date to demonstrate the biocompatibility of MN materials by using the MTT (3-(4,5-Dimethylthiazol-2-yl)-2,5-diphenyltetrazolium bromide, a tetrazole) assay in human epidermal keratinocyte cell lines.

Sullivan et al. (2008) proposed photo-polymerization of poly (vinyl pyrrolidone) (PVP) to fabricate MNs at room temperature (RT). Briefly, a liquid monomer, vinyl pyrrolidone (200 μL), and free-radical initiator, AIBN (azobisisobutyronitile 1.5 wt%) were applied to PDMS molds of MNs (arrays of 15 × 15, 750 μm height, and 250 μm base diameter) and placed under a UV lamp for 30 min at ambient temperatures to induce photo-polymerization. PVP MNs were strong enough to pierce the skin and dissolved within 1 min. To alter the dissolution rate, meth-acrylic acid (MAA) was copolymerized, which produced MNs of greater fracture force and slower dissolution rates within porcine skin in vitro.

Aoyagi et al. (2008) investigated the effectiveness of vibrating a poly (lactic acid) (PLA) MN for ease of insertion, similar to that of the insertion mechanism of the mosquito's proboscis. This study investigated the stress distribution during insertion of a MN in skin using a finite element method (FEM) simulation. Based on FEM simulation, silicon MNs with sharp tip-angle were fabricated, using a wet-etch technique, and replica polymer MNs were created by injection molding. Penetration experiments, in an artificial skin model, showed that using a central-straight shaped MN and two outer jagged ones and a vibrating motion, with tension on the object surface, imitating the mosquito's proboscis, was found to increase ease of insertion.

Han et al. (2009) proposed three-different types of groove-embedded MN shafts with sharp 3D-tips to reduce insertion force, increase fracture force, and increase drug loading within the grooves on the MN. The height, base width, and thickness were 880 ± 20, 710 ± 15, and 145 ± 15 μm, respectively. The grooves-embedded MNs were used to produce PDMS negative molds by a hot embossing process. Array of PLA MNs were fabricated by replicating the negative molds. The mold PLA grains were heated to 190°C and pressed (pressure of 20 kg/cm^2) for 10 min, followed by cooling to room temperature. The grooves-embedded replica MN arrays were then demolded.

Polymeric and carbohydrate MN arrays offer considerable advantages over their metal and silicon counterparts in their ease and economy of preparation and the possibility of being fabricated from biocompatible materials. The possibility of incorporating drug into the matrix of the MN material during preparation also allows for one-step application and avoids problems associated with coating solid MN and blocking of hollow MN. However, addition of drug to hot polymer/carbohydrate melts can cause drug breakdown. MN strength can also be compromised by drug addition and the amount of drug deliverable is necessarily limited to the amount that can be incorporated into the MN and their baseplate.

Consideration of MN design and skin properties

Irrespective of the methods of fabrication described above, MNs should be able to demonstrate sufficent strength to penetrate into the skin or other biological tissue without breaking or bending before or during insertion (Aggarwal & Johnston, 2004). Major factors accountable for MN performance are type of material, needle height, tip-radius, base diameter, needle geometry, needle thickness, and needle density, which, in turn, determine the overall insertion and fracture force of the MN (Davis et al., 2004). Understanding these relationships will allow one to design an ‘intelligent’ or ‘optimized’ MN, with low insertion

force and high fracture force. In doing so, it is necessary to understand the key mechnical properties of the skin, especially that of the *SC* and viable epidermis (*VE*).

Kendall et al. (2007) studied the mechanical properties of skin by penetrating through the intact *SC* and *VE* for efficient targeting of molecules to the immunologically sensitive cells in the viable skin, using micro-nanoprojections on a patch. The study determined the storage modulus, the Young's modulus, and the breaking strength of skin, through the layers of *SC* and *VE* in intact and freshly excised murine skin using a microindentation probe fitted to a NANO-indenter. It was observed that the above-mentioned mechanical properties decreased with depth through the *SC*. The authors indicated that variation in skin properties, such as thickness variation at different body sites, and varitation due to age, sex, race, and body mass index (BMI) needs attention in order to ensure consistent performance of MNs. Laurent et al. (2007) studied the affect of age, race, BMI, gender, and skin thickness variation within the body among 342 adult subjects (205 women, 137 men, 101 Caucasian, 118 Asian, and 123 Black Africans) and evaluated the effciency of ID (intradermal) injection by 1.5 mm long 30G MNs. Results showed that the average skin thickness (epidermis–dermis) was 2.02 mm at deltoid, 2.54 mm at suprascapular, 1.91 mm at waist, and 1.55 mm at thigh regions. Irrespective of the age, race, BMI, or gender the 1.5 mm long MNs could be effeciently used for i.d delivery. Vartiation of *SC* thickness with location on the body, sex, age, and skin condition was also reported by Champion et al. (1998).

The influence of MN geometry on the insertion force and fracture/buckling failure force was first studied by Davis et al. (2004). MN insertion forces (0.1–3 N) varied linearly with interfacial area of needle tip and fracture force increased with increase in the wall thickness, wall angle, and tip radius. However, the saftey margins (i.e. ratio) between fracture force and insertion force were high. Davidson et al. (2008) quantified the influence of different geometrical parameters such as MN thickness, MN diameter, coating depth of drug on MN (i.e. the distance from the tip that is coated by the drug film), penetration depth, spacing between MNs, and array pattern, associated with six different solid MN shapes coated with drug. The aim of the study was to identify the most effective MN geometry for effective skin permeation. The study was performed in a 3D model using FEMLAB scientific modeling software. Depth of penetration and centre-to-centre spacing of MNs were found to significantly affect the effective skin permeability (P_{eff}). On the contrary, the other MN dimensions, such as the diameter of cylindrical MNs, the thickness of flat MNs, and the coating depths, were less significant for P_{eff}. Overall, larger, longer, and more densely packed MNs resulted in greater P_{eff}.

Effective insertion of MN with minimum pain can be accomplished by using a vibratory MN device, controlled by a mechanical actuator, similar to that of the mosquitoe's vibratory (frequency of 200–400 Hz) cutting action. Yang and Zahn (2004) studied the effect of vibratory actuation on MN insertion force. Results showed a significant (greater than 70%) decrease in insertion force by using vibratory actuation. These was due to three-simultaneous factors, i.e. increase in skin's dynamic stiffness, tissue damage by cavitations due to the vibratory waves, and localized thermal damage due to frictional interactions between MN and skin.

Drug incorporation methods for microneedles

The four basic methods of transdermal drug delivery (TDD) mediated by MNs are depicted in Figure 3 (Gill & Prausnitz, 2007a).

In vitro and in vvo drug delivery mediated by MNs

Drug delivery assisted by solid MNs—Solid MNs can be used to mechanically disrupt the *SC* and create transient pores of micron dimensions. In SMNs-based drug delivery, the SMNs are first pressed against the skin's surface, followed by application of traditional patches, containing drug molecules. Molecules of wide-ranging physico-chemical properties have been delivered by using SMNs.

Martanto et al. (2004) used MN arrays (7 × 15) for transdermal delivery of insulin in diabetic rat models. During and after MN treatment, an insulin solution (100 or 500 U/ml) was placed in contact with skin for 4 h. MNs were removed at different times, and blood glucose levels were observed to drop by as much as 80%, an effect similar to that of 1.6–4.1 mU (0.06–0.15 μg) of insulin injected subcutaneously. Chang et al. (2007) developed a built-in roller type MN (230 μm) device, creating 267 holes per cm^2 per single treatment. Following MN roller treatment, the penetration flux of fluorescein isothiocynate (FITC)-labeled ovalbumin, insulin, and bufexame was significantly increased from 13.4 to 83.3, 10.1 to 110.6, and 11.9 to 242.6 pmol/cm^2, respectively. Pearton et al. (2007) evaluated gene delivery by using an array of frustum-shaped silicon MNs (with 4 × 4 array, ≈ 260 μm in height, and ≈ 200 μm base width). It was confirmed that MN application created micro-pores of ≈ 150–200 μm depth on skin and increased the transepidermal water loss (TEWL). Subsequent application of Carbopol®-940 (1% w/v) and thermo-sensitive tri-block copolymer of PLGA-PEG-PLGA (23% w/w) hydrogels, containing known concentration of plasmid DNA (pDNA), was shown to harbor in the micro-conduits created by the MNs and were able to release the pDNA in its functional form for gene expression in the viable tissue.

In an in vitro study, Badran et al. (2009) pre-treated human abdominal skin samples with Dermarollers®, consisting of different MN heights. Invasomes (diameter 100 nm) containing hydrophilic model drugs (radiolabeled mannitol and carboxyfluroescein) were applied to the pre-treated skin samples. Penetration of the model drugs was higher through the Dermaroller® treated skin samples. This was further increased by the invasomes, compared to aqueous solutions of model drugs. Invasomes caused higher penetration, due to their flexibility and penetration-enhancing properties.

Ding et al. (2009) investigated MN-mediated immune responses in a mouse model after transcutaneous immunization using the model antigen diphtheria toxoid (DT). DT, when applied to intact skin, produced low IgG titres. However, MN pre-treated skin showed significantly higher IgG titres, which further increased in the presence of cholera toxin. Recently, Pastorin et al. (2009) used vertically-aligned zinc oxide pyramidal nanorods (nanoneedles), where the tip size was 60 nm and the length less than 50 μm, with a base diameter of 150 nm. The distance between adjacent rods was 300 nm. It was reported that these nanoneedles were sufficient for vaccine delivery and, more importantly, the created nanopores were immediately closed after nanoneedle removal. In addition, we have previously demonstrated the use of solid silicon MN arrays, to enhance skin penetration of 5-aminolevulinic acid (ALA) in vitro and in vivo. Puncturing excised murine skin with 6 × 7 arrays of MNs (270 μm in height, 240 μm in base diameter, and an interspacing of 750 μm) led to a significant (from 178.82 nmol/cm^2h to 427.80 nmol/cm^2h) increase, after 5 h, in transdermal delivery of ALA released from a bioadhesive patch containing 19 mg ALA (cm^{-2}) (Donnelly et al., 2009).

Drug delivery and/or biological fluid sampling mediated by hollow MNs—HMNs consisting of a fine bore can be integrated with a drug solution unit for continuous drug delivery or can be used for biological fluid sampling, unlike the replacement of SMNs with traditional drug-loaded patches for drug delivery.

Martanto et al. (2006a) quantified the relationship between infusion flow rate and other parameters, such as insertion depth (900 and 720 μm), retraction distance (180 μm for every 5 min) (i.e. MN is inserted into the skin to desired depth and then retracted back to desired height), infusion pressure (69 and 172 kPa), needle tipgeometry (bevelled-tip or blunt-tip), tip-opening size (22–48 μm), and presence of hyaluronidase (200 U/ml). The study used a single hollow glass MN, which was attached to a 250 μl or 1 ml glass syringe (containing 1×10^{-3} M sulfurhodamine B solution) and inserted into human cadaver skin. Infusion flow rate was measured with respect to the different parameters mentioned above. It was shown that the insertion/retraction caused a significant increase in flow rate. Increase in pressure was proportional to increase in flow rate. Infusion flow rate was 3-fold greater from a beveled-tip MN than from a blunt-tip MN. Addition of hyaluronidase increased infusion flow rate by 7-fold. Infusion over time caused higher initial flow rates which decayed within a few minutes to a steady state. In contrast to other studies of infusion through hollow MNs, this study demonstrates strategies to increase the flow rate using well-designed infusion protocol and needle geometry. In another study, Martanto et al. (2006b) showed that tissue compaction during the infusion can be avoided by partial retraction, as well as from other approaches, such as MN application via drilling/vibrating motion and insertion at higher velocity. MN retraction caused tissue relaxation, which relieved skin compaction and increased local flow conductivity.

Wang et al. (2000) inserted the same hollow glass MN into the skin of hairless rats in vivo and human cadaver skin in vitro, by using rotary or vibrating penetration devices that drilled the single MN or MN arrays into the skin to known depths. Compounds such as fluorescent calcein, insulin (100 U/ml; Humulin®), FITC-insulin, polymeric microparticles, or Caco-2 intestinal epithelial cells were delivered using hollow MNs and imaged using brightfield or fluorescence microscopy. Histological staining was performed to trace the depth of penetration. The results showed that the rotary drilling of MN into skin can deliver the molecules at a precise depth with low penetration forces. Microinjection of MN to a depth of 800 μm and retracting back to ≈ 200 μm showed increased fluorescent calcein accumulation compared to insertion of MN without retraction. In addition, microinjection of insulin through the MN inserted at a depth of 500–800 μm and infused for 30 min elicited a drop in blood glucose levels by 25% below the pre-treatment values. When the MNs were retracted back by ≈ 200 μm, blood glucose levels were reduced by 75% below pre-treatment values. The experiments also demonstrated efficient microinjection of Caco-2 cells through MNs at rates up to 100 μl/s without loss in cell viability. Higher pressures (2.5–20 psi) were required for delivery of microparticles into the skin. It was also suggested that the vibration of MN arrays can also produce efficient microinjections, similar to the rotary device. Therefore, this study demonstrated that appropriate MN design and insertion protocol can be used to deliver macromolecules, microparticles, and cells precisely to the controlled depth within the skin.

Jiang et al. (2008) used the above glass HMN to overcome the barrier of the eye, the sclera, for ocular drug delivery. Using the above prototype syringe coupled HMN device, the model drug sulforhodamine B, nanoparticles (encapsulated with Nile Red), and microparticles (fluroscein-labeled) were infused in the volumes of 10–35 μl into sclera tissue using individual MNs, where sclera thickness and infusion pressure had insignificant effects on fluid delivery. Therefore, this study demonstrated that the HMNs assisted puncturing of the sclera can facilitate drug diffusion through the sclera into the choroidal and retinal tissues to treat diseases of the posterior of the eye. Patel et al. (2009) recently used the same MNs of 500–1000 μm length to deliver fluids and carboxylate-modified polystyrene nanoparticulate (with diameters of 20, 100, 500, and 1000 nm) suspensions (up to 30 μL) into the suprachorodial space of rabbit, pig, and human eyes.

Verbaan et al. (2007) studied the transport of three different molecules of increasing molecular weight in vitro (cascade blue, M_w = 538 Da, dextran-cascade blue, M_w = 10 kDa, and FITC-dextran, M_w = 72 kDa) across dermatomed human skin. The skin was pre-treated with assembled 4 × 4 arrays of 30 G needles of 300, 550, 700, and 900 μm lengths. A significant increase in the permeation of each of the three compounds was observed for pre-treated skin samples compared to control skin. However, in these studies, the 300 μm length MN arrays were unable to pierce the skin. The skin's natural elasticity resulted in folding of the skin around the 300 μm MNs. Subsequently, to overcome the skin's elasticity, Verbaan et al. (2008) studied the effect of improved piercing by utilizing an electrically-driven applicator with varying velocity (1 and 3 m/s) and compared this to a manual applicator. Verbaan et al. (2008) have also investigated triangular-shaped hollow silicon MNs of ~ 245 μm in length and 250 μm in base, with densities of 4 × 4, 6 × 6, and 9 × 9. Using a velocity of 3 m/s the electric applicator was found superior to a manual applicator in creating conduits on the skin surface in a reproducible manner, for both 245 and 300 μm length MNs. Irrespective of the array density and the type of MNs, the use of the electrically-driven applicator showed a significant increase in the flux of cascade blue through the MN-treated skin when compared to the manual applicator. For example, the flux of cascade blue through manually-pierced skin using the 4 × 4 assembled hollow metal MN array was 9 ± 4 pmol/cm^2/h, whereas the flux was 55 ± 11 pmol/cm^2/h when operated at a velocity of 3 m/s using the electric applicator.

In another study, Nordquist et al. (2007) designed a patch-like integrated MN device (Figure 2c), which was used to deliver insulin to 61 diabetic rats arranged in seven groups. For example, the mean plasma insulin concentration after 210 min of infusion for intravenous (i.v) (0.14 IU/h, 70 IU/ml) administration was 196 ± 20 μIU/ml and for MN-aided intradermal insulin infusion at high-rate (0.40 IU/h, 100 IU/ml) was 167 ± 15 μIU/ml, respectively. It was suggested that this novel concept of intradermal insulin delivery through these integrated MN devices, which not only control the release but are also easy to operate, and may replace the routine subcutaneous (s.c) or i.v insulin therapy.

Drug delivery mediated by coated MNs—Coating of MNs is found to be an attractive technique for rapid bolus delivery of molecules into biological tissue, especially for vaccine delivery to the skin. In addition, coating and drying drug molecules on the surface of MNs may enhance their long-term stability (Gill & Prausnitz, 2007b). Different techniques have been demonstrated for coating MNs with molecules of varying molecular weights. The two most commonly used coating methods for MNs are dip-coating and casting techniques.

Cormier et al. (2004) demonstrated dip-coating of a titanium MN array (Macroflux®) by partial immersion in aqueous solutions of either 24 or 40% of desmopressin and 0.2% of polysorbate 20. Briefly, following coating with different amounts of desmopressin on the MN array (321 MNs/cm^2, area of 2 cm^2, height 200 μm, base-width 170 μm, and thickness 35 μm) the array was affixed to an adhesive patch (patch area 5.3 cm^2) and applied by using a prototype patch applicator. The patch type coated MN array delivered 20 μg of desmopressin within 15 min in a hairless guinea pig model and bioavailability was as high as 85%. Widera et al. (2006), from the same research group, demonstrated dip-coating titanium MN arrays (width 100 μm and 35 μm thickness) with the model antigen ovalbumin (OVA). The number of coatings and concentration of OVA in the coating formulation were used to control the amount of OVA coating onto the MNs. Patches of a variety of tip-shapes and MN density were applied to hairless guinea pig (HGPs) skin in vivo. The influence of depth of vaccine delivery, dose of vaccine delivered, density of MNs, and area of application were investigated. The sera of the immunized HGPs was assessed for the presence of anti-OVA antibodies (IgG), which was determined by an enzyme-linked immunosorbent assay (ELISA). It was observed that the immune response was found to be dose-dependent.

Gill and Prausnitz (2007) designed novel MNs with central openings termed ‘pockets’ (Figure 4a), which were dip-coated with model drugs and various surfactants and viscosity enhancers, prepared in aqueous or organic solvents. It was concluded that coating solutions with lower surface tension facilitated good wetting and decreased speed of film formation on the MN surface. In contrast, higher viscosity caused increased volume of liquid film adherence and residence time to the MN surface. The versatility of this coating technique was demonstrated by coating the hydrophobic molecule, curcumin, and the model proteins, BSA and insulin, in either organic or aqueous-based coating solutions. In addition, a total of up to 1 mg of a model drug, riboflavin, was coated on MN arrays of patch size 10–20 cm^2. A composite filling of the pockets within the MNs was also demonstrated, where multiple coating with more than one drug formulation was achieved with intermittent washing cycles. Gill and Prausnitz (2008) also demonstrated isolation of drugs within the MN pockets and over-coating with another protective layer (e.g. PLGA) followed by a second layer of drug. The pockets could also be filled with liquid drug formulations, which were held in place by surface tension. Using similar stainless steel MNs, Jiang et al. (2007) proposed drug delivery to the eye by using MN of 500–700 μm in length coated with fluorescein and pilocarpine (Figure 4b). The fluorescein coating dissolved within 30 s in an in vitro human cadaveric scleral model. The bioavailability of fluorescein and pilocarpine, when delivered by MNs, was 60- and 45-times higher than that achieved by topical application, respectively, in an in vivo study with rabbit eye.

The grooves-embedded MNs (Type A, Type B, and Type C), as shown in Figure 5, were dip-coated with three different loadings of ovalbumin (1, 10, and 100 μg/ml) and tested for immunization in mouse skin. The degree of immune response was higher in Type C MNs, followed by Type B and A. This result suggests the higher loading capacity of the antigens in the grooves-embedded MNs (Type B and C) than the smooth ones (Type A); therefore, grooves-embedded MNs showed greatest immune response (Han et al., 2009). In a recent study, Kim et al. (2009) investigated the stability, immunogenicity, and protective immunity of vaccine patches comprised of SMNs coated with inactivated influenza virus. SMNs were dip-coated six times in coating solutions containing 15% w/v of trehalose and inserted manually into the skin of anesthetized mice. It was observed that the total antibody (IgG) response was significantly higher for MNs coated with trehalose than without trehalose, which, in turn, was similar to i.m vaccination.

Using a casting method, Xie et al. (2005) coated MN (50–200 μm) with model compounds (calcein and bovine serum albumin, BSA) dispersed in chitosan. Chitosan solution containing these model drugs was poured on the MN chip and allowed to dry overnight at room temperature to form films. The influence of factors, such as matrix thickness, drug content, and matrix concentration was investigated. The in vitro permeation rates of calcein were 50 and 1 $\mu g/cm^2/h$, respectively, with and without MNs. Permeation of BSA increased with decrease in chitosan content and increase in BSA loading; whereas the permeation rate decreased with increase in film thickness.

MN-enhanced TDD can also be achieved by pressing MNs against a skin surface, previously coated with drug solutions. Jae-Ho et al. (2008) used polycarbonate MN arrays (Figure 1c) and investigated the permeation of calcein across excised rat skin in Franz-cell apparatus. A 0.1 g of calcein gel coupled directly with the polycarbonate MNs (500 μm height and154 array cm^{-2}) showed a 5.46-fold increase in permeation after 12 h permeation into the excised rat skin when compared with calcein gel alone. Furthermore, an increase in MN array density from 45 to 154 ea/cm^2 increased the flux of calcein from 30.14 to 54.13 ng cm^{-2} h^{-1} from the calcein gel.

Drug delivery mediated by dissolving MNs—Compared to the other MN application techniques, the major advantage of these types of MNs is the dissolution or bio-degradation of the MN material. Essentially, this type of delivery system depends on the dissolution of MNs upon contact with the skin interstitial fluid. This process (depending upon the MN material) releases the drug molecules from the matrix for local or systemic delivery. To date, most soluble MNs have been manufactured using simple sugars and polymers by using, mostly, molding or casting techniques.

Miyano et al. (2005) were the first to report the production of MNs from natural sugars. Powdered maltose was heated to 140°C for 1 h, to form maltose-candy. Powdered drug was added to this candy and mixed uniformly within a minute and stored in a dry environment at room temperature. Small quantities of this maltose-candy containing drug was then placed onto a casting MN mold at 95°C and cast into MN arrays. Arrays of 500 μm high MNs containing ascorbate-2-glicoside (5% w/w), sodium salicylate (10% w/w), and calcein (10% w/w) were fabricated by this method. MNs were dissolved within a few hours at relative humidities of more than 50%, but retained their shapes for at least 3 months at 40% humidity. Ito et al. (2006a) prepared MNs from a thread-forming biopolymer (dextrin), and the obtained MNs were evaluated for percutaneous delivery of insulin. After administration of these self-dissolving insulin-loaded MNs in mice, dose-dependent hypoglycemic effects were observed and insulin was found to be stable in the MNs for 1 month at 40°C. In MN preparation, poly (propylene) tips were dipped into the dextrin gel and were drawn perpendicularly to form thread-like needles, which were dried at 4°C in a desiccator. Similarly, Ito et al. (2006b) prepared erythropoietin (EPO)-loaded polymeric MNs formed using a thread-forming method for percutaneous administration of EPO in mice. The thread-forming materials used in the present study were dextrin, chondroitin sulfate, and albumin. The relative bioavailability was 82.1, 59.7, and 78.6% for MNs made with dextrin, chondroitin sulphate, and albumin, respectively. In another study, Ito et al. (2008) prepared self-dissolving MNs from dextrin, chondroitin sulphate, or dextran containing lower molecular weight heparin (LMWH) (Mw = 4.5 kDa), where the length and basal diameter of MN was 1.5 mm and 0.5 mm, respectively. At a dose of 100 IU/kg of LMWH, in in vivo studies with rats, the bioavailability was found to be 97.7, 81.5, and 102.3% for dextran, chondroitin, and dextrin MNs, respectively. Furthermore, the content of LMWH loaded in dextran-MNs was found to be stable for at least 3 months when stored at three different conditions, i.e. 40°C, 4°C, and −80°C.

Kolli and Banga (2008) used solid maltose MNs by micro-molding techniques, for instant delivery of nicardipine hydrochloride (NH) across rat skin. Tetrahedron-shaped MNs, with 500 μm heights and 150 μm interspacing, were used to treat rat skin, both in vitro and in vivo. In in vitro Franz-cell diffusion studies (where the donor compartment consisted of 500 μl of 10 mg/ml NH), the MN pre-treated full thickness rat skin showed nearly a 4-fold increase in transdermal penetration of NH compared to passive diffusion. In in vivo studies, the plasma NH level (C_{max}) was 56.45 ng/ml (after ≈ 7 h) for MN treated rats, but detectable levels for passive delivery of NH were seen only after 8 h (with a C_{max} < 20 ng/ml). Similarly, Guohua et al. (2008) studied the effect of similar soluble maltose MNs on the permeation of human immunoglobulin, IgG (Mw = 150 kDa) in rat skin in vitro. The influence of parameters, such as MN length (200 and 500 μm), number of MNs, and drug concentration on in vitro delivery across full thickness rat skin was evaluated. In general, the flux of human IgG increased from 27 to 102 ng/cm^{2}h when needle height changed from 200 μm to 500 μm. Increasing the number of MNs also increased the flux and increasing IgG concentration up to 20 mg/ml increased the flux, after which (for 40 mg/ml) no significant change in flux was noted. This was attributed to the saturation of the boundary layer relative to the donor solution. In contrast, Donnelly et al. (2009a) fabricated API-loaded galactose MNs. Due to high processing temperature (i.e. 160°C) of galactose MNs, substantial losses

of the APIs, namely 5-aminolevulinic acid (ALA) and bovine serum albumin (BSA) was incurred during processing. In vitro drug release experiments using ALA-loaded MN arrays revealed that less than 0.05% of the total drug loading was released across a model silicone membrane. Similarly, only low amounts of ALA (~ 0.13%) and undetectable amounts of BSA were delivered when galactose arrays were combined with aqueous vehicles. Furthermore, galactose MNs were unstable at ambient relative humidities (43% and 83% RH) and became adhesive. Finally, it was suggested by the authors that the carbohydrate-based MNs are not the solution to the problems posed by use of silicon and metal MNs. This is especially true as MNs produced from hot polymer melts also suffer from substantial drug loss during processing.

Park et al. (2006) fabricated beveled-tip MNs from PLGA using a micro-molding technique to encapsulate model drugs (calcein and BSA). Drug molecules were either directly embedded within the PLGA needle matrix (for rapid release) or as a double encapsulation, by first encapsulating the drug within carboxymethylcellulose (CMC) or poly-L-lactide microparticles and then encapsulating the drug-loaded microparticles in the needles (for controlled/delayed release). The diffusion rate of calcein from PLGA-MNs was 1.2×10^{-10} cm^2/s, from CMC microparticle-loaded MNs it was 4.7×10^{-12} cm^2/s, and from PLA microparticle-loaded MNs it was further reduced to 6.2×10^{-10} cm^2/s.

Kwon (2004) proposed a transdermal drug delivery patch, consisting of dissolving MNs. A Generally Regarded As Safe (GRAS) material, sodium carboxymethyl cellulose (SCMC), was loaded with lidocaine HCl and was cast into micromolds, compressed, and then dried to form MNs (550–650 μm in length). In in vitro studies with human cadaver skin, the flux of lidocaine HCl was increased by 4.8-fold from the matrix of the fast-dissolving MNs compared to lidocaine solution (100 mg/ml). In addition, Kwon and Oh (2009) have also shown delivery of parathyroid hormone (PTH) in both in vitro and in vivo studies, in the treatment of bone mass regeneration, using soluble SCMC MNs (1500 μm in height and 670 μm in width). Miyano et al. (2007) developed hydrolytic MNs of maltose and poly (ethylene glycol) (PEG, M_w = 600 Da). The fast-dissolving maltose MNs were one-dimensional tetrahedral MNs with a length of 500 μm and dissolved within 3 h after insertion into skin. However, the high viscosity and low throughput prohibited the fabrication of maltose MNs deployed in 2D-arrays. In contrast, the low viscosity of PEG not only allowed high throughput production of PEG MNs, but also fabrication of 2D-arrays of PEG MNs with length of 1000 or 2000 μm, respectively.

Unlike the typical high-temperature molding or methods which are unsuitable for mass-production of dissolving polymeric MNs, Sullivan et al. (2008) proposed photo-polymerization (UV lamp at 100 W at a wavelength of 300 nm) of liquid monomer, vinyl pyrrolidone. MNs prepared using this method were loaded with 0.2 %w/w Texas Red BSA, which dissolved within 1 min after insertion into pig skin. A dose of 1 mg of β-galactosidase when encapsulated within MNs maintained enzymatic activity similar to a solution of β-galactosidase in PBS.

Jeong et al. (2008) proposed encapsulated molecules within pyramidal MNs, which dissolve in the skin for bolus or sustained release over time (168 h) was observed when molecules were encapsulated in the backing layer of MN. MNs were made from carboxymethylcellulose (CMC), amylopectin (AP), and bovine serum albumin (BSA) using casting techniques. Model drugs, sulforhodamine B (0.15–30%w/w), BSA (20%w/w), and lysozyme (5%w/w) were either encapsulated in MN or the backing layer or both for skin insertion and release studies. For example, Figure 6b shows the release of sulforhodamine B after the dissolution of CMC MNs (Figure 6a) over time. The mechanical properties of the MNs (600 μm height, 300 μm base width, and 600 μm spacing) were ranked from strongest

to weakest as: AP, CMC/BSA (80/20 wt%), BSA, and CMC. Interestingly, encapsulated lysozyme was found to be stable for 2 months at room temperature.

Drug delivery mediated by combination of MNs and other techniques—A range of other enhancing techniques in combination with MNs has also been investigated to further enhance drug delivery through MN-induced micropores. The synergistic effect of MN and iontophoresis (ITP), nanoparticles, or both have been recently investigated.

Wu et al. (2007) studied the combined effect of MN pre-treatment and ITP on in vitro permeability of low molecular weight D_2O and high molecular weights of FITC-dextrans, with average molecular weights of ≈ 4, 10, 39, 71, and 200 kDa, respectively. Results indicated that the passive permeation of D_2O was almost similar to that of the combined effect of MN and ITP, whereas a significant increase in flux of FITC-dextrans, was observed when MNs and ITP were used together. However, permeation decreased with increase in the MW of the FITC-dextrans. Vemulapalli et al. (2008) investigated the synergistic effect of ITP and soluble maltose MNs (two-rows of 28 MNs each of 500 μm in height) on the permeation of methotrexate (MTX). In in vivo studies in rats, it was shown that the combined effect of MNs and ITP caused a 25-fold increase in the MTX delivery, when compared to either MNs or ITP alone. Katikaneni et al. (2009) used the same maltose MNs (six-rows of 27 needles each) in combination with ITP for the delivery of a high molecular weight protein, daniplestim (M_w 12.76 kD). A significant increase in the permeability of daniplestim from 0 to 718 ng/cm^2 (in TRIS buffer at pH 7.5) and from 555 to 22,728 ng/cm^2 (in acetate buffer at pH 4.0) was observed.

Chen et al. (2009) showed in vitro permeation of insulin nanovesicles, of various zeta potential, and diameters. Penetration of insulin nanovesicles through guinea pig skin was significantly higher than an insulin solution in PBS, which could not penetrate. This was because the soybean lecithin in the nanovesicles caused disruption of lipid structures of the skin and, thereby, enhanced insulin delivery. However, the nanovesicles could not deliver clinically-effective amounts of insulin. In contrast, MN-induced microchannels in combination with ITP showed efficient permeation of insulin. Permeation rates of insulin from positive nanovesicles driven by ITP through skin with MN-induced microchannels were 713.3-times higher than that of its passive diffusion. Furthermore, in vivo studies in diabetic rats showed a similar effect to that of s.c injections in controlling blood glucose levels. Qiu et al. (2008) investigated a combination method of MN pre-treatment and elastic liposomes to increase skin permeation of docetaxel (DTX, M_w = 807.9) in in vitro models. DTX liposomal systems with and without elastic properties were prepared and characterized. Elastic liposomes significantly improved skin delivery of DTX compared to conventional liposomes and the saturated 20% w/w ethanolic solution control without MN treatment. Permeation of elastic liposomes through skin, previously treated with MN, reduced the lag time by nearly 70% compared with that obtained from conventional liposomes.

Human studies to demonstrate the clinical safety and efficacy of MN application

Even though MN technology has been shown to enhance transmembrane delivery of a wide range of molecules, as demonstrated in both in vitro and ex vivo models, only a few studies have reported the success of such devices in human subjects.

Kaushik et al. (2001) carried out the first human study, consisting of 12 male and female healthy volunteers aged between 18–40 years to show that MN application was painless. MNs used in this study were 150 μm long with a base diameter of 80 μm and tip radius of 1

μm. Each array contained a total of 400 MNs. Pain-scores from the subjects were recorded on a visual analog scale (VAS), and it was found that MN application was painless and caused no skin damage or irritation. Bal et al. (2008) investigated safety and barrier disruption following application of MN arrays of different lengths and types, in 18 healthy volunteers (nine men and nine women) aged between 21–30 years. Parameters such as barrier function of skin (measured by the TEWL), erythema (evaluated by skin color and Laser Doppler imaging (LDI) methods), and pain-score were measured. TEWL and erythema values after treatment with solid MN arrays of 400 μm height were significantly increased compared to 200 μm. However, for all MNs, irritation was short-lasting (< 2 h) and application was painless.

Sivamani et al. (2005) studied injection of methyl nicotinate in 11 healthy human subjects, using an array of either pointed or symmetric HMNs, made from silicon (200 μm long and 40 μm lumen diameter) and glued to a syringe. It was observed that the pointed MN injections resulted in higher blood flux than the symmetric MNs. Volunteers reported feelings of pressure, but no pain during MN application. The same workers also investigated whether the hollow silicon MN arrays were capable of penetrating and delivering drugs past the *SC* in five human volunteers (Sivamani et al., 2007). Hexyl nicotinate (HN), a lipophilic vasodilator, used as a marker of *SC* penetration, was either injected or applied topically at tape-stripped and unstripped sites of the forearms. Measuring the blood flow by Laser Doppler imaging (LDI) it was demonstrated that MNs were capable of injecting the drug beyond the *SC*. Furthermore, tape-stripping did not significantly benefit MN penetration, indicating that MNs bypass the *SC* barrier. Haq et al. (2009) investigated the pain (usinga 0–10 cm VAS score) and sensory responses (using McGill Pain Questionnaire Short Form) in 12 human subjects. The subjects received insertion of two-different types of silicon MNs (of 180 and 280 μm heights and in 6 × 6 arrays) and a 25-G hypodermic needle. The mean VAS pain scores were ≈ 0.25 and ≈ 0.60 cm for 180 and 280 μm MN heights, respectively. VAS scores for subjects treated with hypodermic needle were ≈ 1.25 cm. Furthermore, participants felt greater ‘sharp’ and ‘stabbing’ sensations with hypodermic needles, and more ‘pressing’ and ‘heavy’ sensations when the MNs were applied. A methylene blue staining study showed that the MN-induced micropores close at 8–24 h after the removal of MNs immediately.

Wermeling et al. (2008) conducted the first clinical studies in human subjects to demonstrate the MN-based transdermal delivery of a hydrophilic compound, naltrexone (NTX). MNs used in the current study were 620 μm in height, 160 μm in width, and in 5 × 10 arrays. NTX adhesive patches were applied to the upper arm after treating with MNs and blood samples were collected over 72 h. Results showed rapid absorption (1.6–8.1 ng/ml) of NTX within the first few hours of application, followed by steady-state plasma concentrations of ≈ 2.5 ng/ml over 72 h.

Damme et al. (2009) conducted a single-blinded study to evaluate the safety and immunogenicity of intradermal delivery of low-dose influenza vaccines (α-RIX®), using a novel MN device in 180 healthy men and women (aged 18–40 years). The MN device (MicronJet™) consisted of an array of 4-silicon MNs (450 μm length) bonded to the tip of a plastic adapter which, in turn, can be mounted on any standard syringe. Subjects were randomly assigned to receive either a full-dose intramuscularly (IM) (15 μg hemagglutinin (HA) per strain) by conventional needle (IM group) or a low-dose intradermally (ID1 group) (3 μg HA per strain) by MicronJet™ or medium-dose intradermally (ID2 group) (6 μg HA per strain) by MicronJet™. It was concluded that the low-dose influenza vaccines delivered by MicronJet™ produced immunogenicity responses similar to that of full dose IM vaccinations. Gupta et al. (2009) tested the efficiency of hollow MN in delivery of insulin in Type 1 diabetic adults (one male and one female) compared to that of a catheter infusion set

(9 mm). MN were attached to a 3 ml syringe which was further connected to a syringe pump that controlled the insulin delivery rate. MN were inserted at a 90° angle into the abdominal skin at depths ranging from 1–5 mm using a custom-made rotator device. Results showed that the MN insertion depth of 1 mm within the skin led to rapid insulin absorption and reduction in glucose levels in fasting subjects. It was also found that MNs inserted 1 mm into skin were effective in reducing pos-tprandial glucose levels. Subjects reported no pain following MN application.

Even though fewer studies have addressed safety of MN application, potential for microbial permeation into the viable epidermis through the micron-sized pathways created by these MNs was not reported. Nevertheless, we have very recently demonstrated that the microorganisms (i.e. *Candida albicans*, *Pseudomonas aeruginosa*, and *Staphylococcus epidermidis*) can traverse through the MN-induced holes in the *stratum corneum*. However, the infection risk associated with skin application of MNs is minimal and likely to be less than that associated with hypodermic needles. Safety can be enhanced by aseptic or sterile manufacture and by fabricating MNs from self-disabling materials (e.g. dissolving or biodegradable polymers) to prevent inappropriate or accidental reuse (Donnelly et al., 2009b).

Microneedle applicators for drug delivery

Unlike the application of traditional patch-based delivery systems, the application of MNs requires the assistance of external energy to ensure efficient penetration of MNs into biological tissue at desired depths. This assistance can be by either utilizing an applicator device, which serves the function of presenting the MN arrays to the biological tissue, such as skin, or by using a manual application method. Understandably, it is difficult to produce consistent penetration depths and uniform pressures by manual application methods. In contrast, applicator devices can provide consistent penetration into biological tissue, with minimum inter-individual variability. MN arrays can either be integrated within an applicator device which, upon activation, can deliver the MN array into the skin surface, or the MN arrays can be applied to the skin and the device then activated to push the MN through the *SC*. The literature shows that these types of applicators are for either single-use or multiple-use.

Recently, various applicator designs have been disclosed, but many are in their development stage. The simplest type of single-use disposable applicator termed 'MicroCor™' was presented by Corium international Ltd (Menlo Park, CA, USA). In this system, the MNs are present under the surface, as shown in Figure 7a. The applicator is applied with light finger pressure and worn for a few minutes or less and removed. Drug delivery could be quick or continuous depending on MN formulation (Cleary, 2009). Zosano's Macroflux® transdermal microprojection delivery system allows administration of therapeutic molecules from coated MNs patches, which are designed to be stable at ambient conditions (Figure 7b-i). The reusable-applicator consists of an integrated MN-loaded adhesive patch which, upon activation by pressing against skin surface (Figure 7b-ii), delivers the patch at the site of application (Figure 8b-iii) (Zosanopharma, 2009).

NanoBioSciences LLC has developed a proprietary MN shape termed Advanced micro-needle Patch (ADMIN PATCH®) MN array (Figure 7c). The claimed advantages of this design are that the shape of the MN allows continuous delivery of drugs when inserted in the skin. The MNs are formed from a standard metal film, which allows very robust and inexpensive manufacture, and a conventional transdermal drug-in-adhesive patch can be simply laminated on the back surface of the ADMINPATCH® MN array (Nanobiosciences, 2009).

NanoPass Technologies Ltd designed the MicronJet® MN device, which consists of hollow type MNs mounted on a standard syringe barrel. This system requires minimal expertise for intradermal delivery of therapeutic molecules (Figure 7d). The MicronJet® MN device contains an array of 'MicroPyramids', each less than 500 μm high (Nanopass, 2009). Similarly, BD Soluvia™ described a prefillable microinjection system that is integrated with a miniature BD™ MN (Figure 7e). This device is similar in appearance to hypodermic syringes. However, the needle height is much shorter (BD, 2009). BD Soluvia™ claim that the MN system is barely perceptible, safe, easy to use, and showed reproducible injections to the dermal layer, irrespective of the subject's gender, age, ethnicity, and body mass (Laurent et al., 2007a; b).

The Microneedle Therapy System (MTS)-Rollers™ from Clinical Resolution Laboratory Inc. (LA, USA) uses steel MNs with heights ranging from 0.2–2.0 mm mounted onto radial discs. The discs are held together with the help of handle (Figure 7f). This discs-integrated MN roller is then rolled over the skin surface to produced micropores. This technology is, at present, available in different models, such as for personal use, for medical use, and for clinical use. They are used in treating alopecia, skin 'restoration', active ingredient delivery, and various other cosmetic applications (Microneedle, 2009). Similar to the MTS-Rollers™, Nanogen is marketing Scalproller™, a specially designed roller to help treat thinning hair. The Scalproller™ uses titanium needles unlike the steel needles used in MTS-Rollers™ (Nanogen, 2009).

Conclusion

MN application has the potential to overcome the problems associated with delivery of small hydrophilic molecules, macromolecules, and biopharmaceuticals across biological barriers, particularly the *SC*. Given the potential of such agents as next-generation therapeutics, it is hardly surprising that a significant number of firms are actively involved in fabrication and evaluation of MN devices (Donnelly et al., 2007; Thakur et al., 2010). Indeed, it is now well known that MN-based drug delivery techniques, and combinations thereof, can enable successful delivery of a wide range of drug molecules.

In this review we have summarized the work done by various research groups in this area. MNs of various designs have been fabricated using different techniques. However, not all of them have the ability to produce the desired enhancement in delivery of the molecule of interest. A wide variety of variables, such as height, density, aspect ratio, type of material, patch size, and duration of application related to MNs may affect drug transport. To understand the effect of these variables on skin permeability, researchers have proposed different theories. Stoeber and Liepmann (2005) suggested that the length of the MN must be longer than 100 μm to overcome the skin's flexibility and permit efficient penetration. In contrast, Shikida et al. (2006) defined the ideal MN length to be longer than 50 μm but shorter than 200 μm, and Pastorin et al. (2009) suggested that MNs of a length below 50 μm can efficiently enhance skin permeability and do not cause pain. Teo et al. (2006) studied a number of MN geometires, such as straight-walled solid MNs, straight-walled hollow MNs, and solid MNs with sharp tips. Despite the sharpness of the tips, it was suggested that insertion of needles by hand is difficult and not very consistent. Al-Qallaf et al. (2007) used mathematical models and studied the effect of duration of MN application, MN length, MN patch surface area, skin thickness, and pharmacokinetic variables on the transport of fentanyl and human growth hormone. Al-Qallaf and Das (2008; 2009) also proposed an optimization model for improving drug permeability in skin. Optimized designs for both solid and hollow MNs was proposed, in which higher skin permeability was observed when the aspect ratio of needle height over needle radius was decreased and the number of MNs was increased. Skin thickness was found to strongly effect the skin's permeability for

different skin types (e.g. different race, sex, age, and anatomical regions). However, this theoretical model needs to be experimentally validated. Ideally, the utility of a particular type of MN needs to be clearly demonstrated in in vitro experiments, followed by a sufficient number of in vivo experiments.

Even though safety of MNs has been investigated to some extent, comprehensive additional clinical studies are now necessary to show that creation of pores in biological membranes is safe and reversible and does not cause microbial infection. Equally important is MN-applicator design. This will undoubtedly be vital if MN-based drug delivery systems are to gain widespread clinical and patient acceptance, since a patient should be able to apply the device without assistance in their own home. One of the major selling points of conventional transdermal patches is their ease of use. MN-applicators should be available at relatively low cost, be reusable, and be easily handled by all patients.

References

Adams, AC. Dielectric and polysilicon film deposition. In: Sze, SM., editor. VLSI technology. McGraw-Hill; New York: 1988. p. 233-71.

Aggarwal P, Johnston CR. Geometrical effects in mechanical characterizing of microneedle for biomedical applications. Sens Actuators B 2004;102:226–34.

Al-Qallaf B, Das DB. Optimization of square microneedle arrays for increasing drug permeability in skin. Chem Eng Sci 2008;63:2523–35.

Al-Qallaf B, Das DB. Optimizing microneedle arrays to increase skin permeability for transdermal drug delivery. Ann N Y Acad Sci 2009;1161:83–94. [PubMed: 19426308]

Ambrose CG, Clanto TO. Bioabsorbable implants: review of clinical experience in orthopedic surgery. Ann Biomed Eng 2004;32:171–7. [PubMed: 14964733]

Aoyagi S, Hayato I, Mitsuo F. Biodegradable polymer needle with various tip angles and consideration on insertion mechanism of mosquito's proboscis. Sens Actuators A Physical 2008;143:20–8.

Aoyagi S, Hayato I, Yuichi I, Mitsuo F, Ogawa H. Laser fabrication of high aspect ratio thin holes on biodegradable polymer and its application to a microneedle. Sens Actuators A Physical 2007;139:293–302.

Arduino MJ, Bland LA, Danzig LE, McAllister SK, Aguero SM. Microbiologic evaluation of needleless and needle-access devices. Am J Infect Contr 1997;25:377–80.

Arora A, Prausnitz MR, Mitragotri S. Micro-scale devices for transdermal drug delivery. Int J Pharm 2008;364:227–36. [PubMed: 18805472]

Badran MM, Kuntsche J, Fahr A. Skin penetration enhancement by a microneedle device (Dermaroller®) in vitro: dependency on needle size and applied formulation. Eur J Pharm Sci 2009;36:511–23. [PubMed: 19146954]

Bal SM, Caussin J, Pavel S, Bouwstra JA. In vivo assessment of safety of microneedle arrays in human skin. Eur J Pharm Sci 2008;35:193–202. [PubMed: 18657610]

Banga AK. Photolithography. In: Microporation applications for enhancing drug delivery. Expert Opin Drug Deliv 2009;6:343–54. [PubMed: 19348604]

Banks, D. Microengineering, MEMS, and interfacing. A practical guide. CRC, Taylor and Francis; Boca Raton: 2009. p. 21-72.

BDAvailable online at: http://www.bd.com/pharmaceuticals/products/microinjection.asp, accessed 1 October 2009

Bin M, Sheng L, Zhiyin G, Guojun L, Xinxia C, Honghai Z, Zhigang Y. A PZT insulin pump integrated with a silicon microneedle array for transdermal drug delivery. Microfluid Nanofluid 2006;2:417–23.

Braybrook, JH. Biodegradation and Toxicokinetic Studies. In: Braybrook, JH., editor. Biocompatiblity: Assessment of medical devices and materials. Wiley; New York: 1997. p. 97-109.

Champion, RH.; Burton, JL.; Tony, B.; Stephen, B. Textbook of dermatology. In: Jeffrey, D., editor. 6th ed.. Wiley-Blackwell; Bernhard. Massachusetts: 1998. p. 231-340.

Chandrasekaran S, Brazzle JD, Frazier AB. Surface micromachined metallic microneedles. J MEMS 2003;12:281–8.

Chandrasekaran, S.; Frazier, AB. Characterization of surface micromachined metallic microneedles; MEMS IEEE 16th Annual Int Conference, JMEMS; 2003. p. 289-295.

Chang RL, Moon SK, Lee HB, Han KL, John MR, Gilson K. The effect of molecular weight of drugs on transdermal delivery system using microneedle device. Key Eng Mater 2007;342/3:945–8.

Chen H, Zhu H, Zheng J, Mou D, Wan J, Zhang J, Shi T, Zhao Y, Xu H, Yang X. Iontophoresis-driven penetration of nanovesicles through microneedle-induced skin microchannels for enhancing transdermal delivery of insulin. J Contr Rel 2009;139:63–72.

Clark, LD.; Edell, DJ. KOH:H_2O etching of (110) Si, (111) Si, SiO_2, and Ta: an experimental study; Proceedings of the IEEE Micro Robots and tele-operators workshop; Hyannis, MA. 1987. p. 5/1-6.

Cleary, GW. The Emergence of Active Transdermal Drug Delivery. Control Release Society Presentation; Copenhagen, Denmark. July 18-22nd; 2009.

Cormier M, Johnson B, Ameri M, Nyam K, Libiran L, Zhang D, Daddona P. Transdermal delivery of desmopressin using a coated microneedle array patch system. J Contr Rel 2004;97:503–11.

Daddona P. Macroflux® transdermal technology development for the delivery of therapeutic peptides and proteins. Drug Deliv Tech 2002:2.

Damme PV, Froukje OK, Van der MW, Almagor Y, Sharon O, Levin Y. Safety and efficacy of a novel microneedle device for dose sparing intradermal influenza vaccination in healthy adults. Vaccine 2009;27:454–9. [PubMed: 19022318]

Davidson A, Al-Qallaf B, Bhusan DD. Transdermal drug delivery by coated microneedles: geometry effects on effective skin thickness and drug permeability. Chem Eng Res Design 2008;86:1196–206.

Davis SP, Landis BJ, Adams ZH, Allen MG, Prausnitz MR. Insertion of microneedles into skin: measurement and prediction of insertion force and needle fracture force. J Biomechanics 2004;37:1155–63.

Davis SP, Martanto W, Allen MG, Prausnitz MR. Hollow metal microneedles for insulin delivery to diabetic rats. IEEE Trans Biomed Eng 2005;52:909–15. [PubMed: 15887540]

Dean CH, Alarcon JB, Waterston AM, Draper K, Early R, Guirakhoo F, Monath TP, Mikszta JA. Cutaneous delivery of a live, attenuated chimeric flavivirus vaccine against Japanese encephalitis (ChimeriVax-JE) in non–human primates. Hum Vaccines 2005;1:106–11.

Ding Z, Verbaan FJ, Bivas BM, Bungener L, Huckriede A, Van den Berg DJ, Kersten G, Bouwstra JA. Microneedle arrays for the transcutaneous immunization of diphtheria and influenza in BALB/c mice. J Contr Rel 2009;136:71–8.

Donnelly RF, Morrissey A, McCarron PA, Woolfson DA. Microstructured devices for transdermal drug delivery and minimally-invasive patient monitoring. Recent Pat Drug Deliv Formul 2007;1:195–200. [PubMed: 19075886]

Donnelly RF, Morrow DI, McCarron PA, Woolfson AD, Morrissey A, Juzenas P, Juzeniene A, Iani V, McCarthy HO, Moan J. Microneedle-mediated intradermal delivery of 5-aminolevulinic acid: potential for enhanced topical photodynamic therapy. J Control Release 2008;129:154–62. [PubMed: 18556084]

Donnelly RF, Morrow DIJ, Singh TRR, Migalska K, McCarron PA, O'Mahony C, Woolfson AD. Processing difficulties and instability of carbohydrate microneedle arrays. Drug Dev Ind Pharm 2009a;35:1242–54. [PubMed: 19555249]

Donnelly RF, Singh TRR, Tunney MM, Morrow DI, McCarron PA, O'Mahony C, Woolfson AD. Microneedle arrays allow lower microbial penetration than hypodermic needles in vitro. Pharm Res 2009b;26:2513–22. [PubMed: 19756972]

Down, JA.; Harvey, NG. Minimally invasive systems for transdermal drug delivery. In: James, A.; Guy, RH.; Hadgraft, J., editors. Transdermal drug delivery. Marcel Dekker Inc; New York: 2003. p. 327-60.

Gary, C. The Emergence of Active Transdermal Drug Delivery; Controlled Release Society Annual Meeting; Copenhagen, Denmark. 18-22 July; 2009.

Gerstel, MS.; Place, VA. US patent US3964482. 1976.

Gill HS, Prausnitz MR. Coated microneedles for transdermal delivery. J Contr Rel 2007a;117:227–37.

Gill HS, Prausnitz MR. Coating formulations for microneedles. Pharm Res 2007b;24:1369–1380. [PubMed: 17385011]

Gill HS, Prausnitz MR. Pocketed microneedles for drug delivery to the skin. J Phys Chem Solids 2008;69:1537–41.

Guohua L, Badkar A, Sandeep N, Kolli CS, Banga AK. In vitro transdermal delivery of therapeutic antibodies using maltose microneedles. Int J Pharm 2008;368:109–15. [PubMed: 18996461]

Gupta J, Felner EI, Prausnitz MR. Minimally invasive insulin delivery in subjects with type 1 diabetes using hollow microneedles. Diabetes Technol Ther 2009;11:329–37. [PubMed: 19459760]

Han M, Hyun DH, Park HH, Lee SS, Kim CH, Kim CG. A novel fabrication process for out-of-plane microneedle sheets of biocompatible polymer. J Micromech Microeng 2007;17:1184–91.

Han M, Kim DK, Seong HK, Yoon HR, Kim BY, Lee SS, Kim KD, Lee HG. Improvement in antigen-delivery using fabrication of a grooves-embedded microneedle array. Sens Actuators B 2009;137:274–80.

Haq MI, Smith E, John DN, Kalavala M, Edwards C, Anstey A, Morrissey A, Birchall JC. Clinical administration of microneedles: skin puncture, pain and sensation. Biomed Microdevices 2009;11:35–47. [PubMed: 18663579]

Hashmi S, Ling P, Hashmi G, Reed M, Gaugler R, Trimmer W. Genetic transformation of nematodes using arrays of micromechanical piercing structures. BioTechniques 1995;19:766–70. [PubMed: 8588914]

Henry S, McAllister DV, Allen MA, Prausnitz MR. Microfabricated microneedles: a novel approach to transdermal drug delivery. J Pharm Sci 1998;87:922–5. [PubMed: 9687334]

Ito Y, Eiji H, Atsushi S, Nobuyuki S, Kanji T. Feasibility of microneedles for percutaneous absorption of insulin. Eur J Pharm Sci 2006a;29:82–8. [PubMed: 16828268]

Ito Y, Jun-Ichiro Y, Keiji S, Nobuyuki S, Kanji T. Self-dissolving microneedles for the percutaneous absorption of EPO in mice. J Drug Target 2006b;14:255–61. [PubMed: 16882545]

Ito Y, Murakami A, Maeda T, Sugioka N, Takada K. Evaluation of self-dissolving needles containing low molecular weight heparin (LMWH) in rats. Int J Pharm 2008;349:124–9. [PubMed: 17826015]

Jae-Ho O, Park HH, Ki-Young DO, Han M, Hyun DH, Kim CG, Kim CH, Lee SS, Sung-Joo H, Shin SC, Cho CW. Influence of the delivery systems using a microneedle array on the permeation of a hydrophilic molecule, calcein. Eur J Pharm Biopharm 2008;69:1040–5. [PubMed: 18411045]

Jason BA, Andrea WH, Harvey NG, Mikszta JA. Preclinical evaluation of microneedle technology for intradermal delivery of influenza vaccines. Clin Vacc Immun 2007;14:375–81.

Jensen, KF. Chemical vapor deposition. In: Hess, DW.; Jensen, KF., editors. Microelectronics processing: Chemical engineering aspects. American Chemical Society; Washington, DC: 1989. p. 199-264.

Jeong WL, Park JH, Prausnitz MR. Dissolving microneedles for transdermal drug delivery. Biomaterials 2008;29:2113–24. [PubMed: 18261792]

Jiang J, Gill HS, Deepta G, McCarey BE, Samir RP, Henry FE, Prausnitz MR. Coated microneedles for drug delivery to the eye. Invest Ophthal Visual Sci 2007;48:4038–43. [PubMed: 17724185]

Jiang J, Moore JS, Henry FE, Prausnitz MR. Intrascleral drug delivery to the eye using hollow microneedles. Pharm Res 2008;26:395–403. [PubMed: 18979189]

Jing, J.; Francis, EHT.; Jianmin, M.; Ciprian, I. Microfabricated silicon microneedle array for transdermal drug delivery; J Phys Conf Series, Int MEMS Conf; 2006. p. 1127-31.

Katikaneni S, Badkar A, Nemab S, Banga AK. Molecular charge mediated transport of a 13 kD protein across microporated skin. Int J Pharm 2009;378:93–100. [PubMed: 19501142]

Katsuma S, Tsujimoto G. Genome medicine promised by microarray technology. Expert Rev Molec Diagnos 2001;1:377–82.

Kaushik S, Allen HH, Donald DD, McAllister DV, Smitra S, Allen MG, Prausnitz MR. Lack of pain associated with microfabricated microneedles. Anesth Analg 2001;92:502–4. [PubMed: 11159258]

Kendall MAF, Chong YF, Alexander C. The mechanical properties of the skin epidermis in relation to targeted gene and drug delivery. Biomaterials 2007;28:4968–77. [PubMed: 17720240]

Kern W. Chemical etching of silicon, germanium, gallium, arsenide, and gallium phosphide. RCA Rev 1978;39:278–308.

Kim YC, Quan FS, Richard WC, Kang SM, Prausnitz MR. Improved influenza vaccination using coated microneedles. Controlled Release Society. July 18-22;2009

Kolli CS, Banga AK. Characterization of solid maltose microneedles and their use for transdermal delivery. Pharm Res 2008;25:104–13. [PubMed: 17597381]

Kwon, SY. In vitro evaluation of transdermal drug delivery by a micro-needle patch; Controlled Release Society 31st Annual Meeting Transactions; TheraJect Inc.; 2004. no.115

Kwon SY, Oh SJ. In vitro and in vivo transdermal PTH delivery by a dissolving micro-needle patch. CRS. July 18-22;2009

Laurent A, Mistretta F, Bottigioli D, Karima D, Catherine G, Jean FN, Anca H, Philippe EL. Echographic measurement of skin thickness in adults by high frequency ultrasound to assess the appropriate microneedle length for intradermal delivery of vaccines. Vaccine 2007;25:6423–30. [PubMed: 17640778]

Laurent P, Stephane B, Paul A, Paulina R, John AM, Ronald P. Evaluation of the clinical performance of a new intradermal vaccine administration technique and associated delivery system. Vaccine 2007a;25:8833–42. [PubMed: 18023942]

Le Barny, P. Chemistry of polymer molecules for ultrathin films. In: Stroeve, P.; Franses, E., editors. Molecular engineering of ultrathin polymeric films. Elsevier; New York: 1987. p. 325-76.

Leoni L, Desai TA. Micromachined biocapsules for cell-based sensing and delivery. Adv Drug Deliv Rev 56:211–29. [PubMed: 14741117]

Lindner D. Microsystems for chemical and biological applications. MRS Bull 2001;26:333–6.

Lippmann JM, Geiger EJ, Pisano AP. Polymer investment molding: Method for fabricating hollow, microscale parts. Sensors and Actuators A: Physical 2007;134:2–10.

Madou, MJ. Lithography. In: Madou, Marc J., editor. Fundamentals of microfabrication: the science of miniaturization. 2nd ed.. CRC; Boca Raton: 1997. p. 1-71.

Martanto W, Davis SP, Nicholas RH, Wang J, Gill HS, Prausnitz MR. Transdermal delivery of insulin using microneedles in vivo. Pharm Res 2004;21:947–52. [PubMed: 15212158]

Martanto W, Moore JS, Couse T, Prausnitz MR. Mechanism of fluid infusion during microneedle insertion and retraction. J Contr Rel 2006b;112:357–61.

Martanto W, Moore JS, Kashlan O, Kamath R, Wang PM, O'Neal JM, Prausnitz MR. Microinfusion using hollow microneedles. Pharm Res 2006a;23:104–13. [PubMed: 16308670]

Matteucci M, Fanetti M, Casella M, Gramatica F, Gavioli L, Tormen M, Grenci G, De Angelis F, Fabrizio ED. Poly vinyl alcohol re-usable masters for microneedle replication. Microelect Eng 2009;86:752–6.

McAllister DV, Allen MG, Prausnitz MR. Microfabricated microneedles for gene and drug delivery. Annu Rev Biomed Eng 2000;2:289–313. [PubMed: 11701514]

McAllister DV, Wang PM, Davis SP, Park JH, Canatella PJ, Allen MG, Prausnitz MR. Microfabricated needles for transdermal delivery of macromolecules and nanoparticles: Fabrication methods and transport studies. PNAS 2003;100:13755–60. [PubMed: 14623977]

MEMSnet. Avilable online at: http://www.memsnet.org/mems/processes/, accessed 2 October 2009

Metz TE, Savage RN, Simmons HO. In situ control of photoresist coating process. Semicond Int 1992;15:68–9.

Microneedle. 2009. Available online at: http://www.microneedle.com/main/index.html, accessed 1 October 2009

Mikszta, JA.; Haider, MI.; Pettis, RJ. Microneedle for drug and vaccine delivery: when will the dream become a reality?. In: Wille, JJ., editor. Skin delivery systems: Transdermals, dermatologicals, and cosmetic actives. Blackwell Publishing; Iowa: 2006. p. 309-25.

Miyano, T.; Miyachi, T.; Okanishi, T.; Todo, H.; Sugibayashi, K.; Uemura, T.; Takano, N.; Konishi, S. Hydrolyticmicroneedles as transdermal drug delivery system; Solid-state sensors, actuators and microsystems conference; Lyon, France. Transducers. International. January 1 2007; 2007.

Miyano T, Tobinaga Y, Takahiro K, Matsuzaki Y, Hitoshi T, Makoto W, Katsumi H. Sugar micro needles as transdermic drug delivery system. Biomed Microdevices 2005;7:185–8. [PubMed: 16133805]

Moon SJ, Lee SS. A novel fabrication method of a micro-needle array using inclined deep x-ray exposure. J Micromech Microeng 2005;15:903–11.

Moon SJ, Lee SS, Lee HS, Kwon TH. Fabrication of microneedle array using LIGA and hot embossing pocess. Microsyst Technol Micro Nanosyst Informat Storage Proc Syst 2005;11:311–8.

Moreau, WM. Semiconductor lithography. Plenum press; New York: 1988. p. 88

Mukerjee EV, Collins SD, Isseroff RR, Smith RL. Microneedle array for transdermal biological fluid extraction and in situ analysis. Sens Actua A Physical 2004;114:267–75.

Nanobiosciences. 2009. Available online at: http://www.nanobiosciences.com/, accessed 1 October 2009

Nanogen. 2009. Available online at: http://nanogen.co.uk/nanogenscalproller-hair-growth-stimulator.html

Nanopass. 2009. Available online at: http://www.nanopass.com/content-d.asp?tcid=19&cid=24, accessed 1 October 2009

Nordquist L, Roxhed N, Griss P, Stemme G. Novel microneedle patches for active insulin delivery are efficient in maintaining glycaemic control: an initial comparison with subcutaneous administration. Pharm Res 2007;24:93–100.

Ovsianikov A, Chichkov B, Mente P, Monteiro-riviere NA, Doraiswamy A, Narayan RJ. Two photon polymerization of polymer-ceramic hybrid materials for transdermal drug delivery. Int J Appl Ceramic Tech 2007;4:22–9.

Paik SJ, Sangwon B, Lim JM, Park Y, Lee A, Chung S, Changa J, Chuna K, Cho DD. In-plane single-crystal-silicon microneedles for minimally invasive microfluid systems. Sens Actua A 2004;114:276–84.

Park JH, Allen MG, Prausnitz MR. Biodegradable polymer microneedles: fabrication, mechanics and transdermal drug delivery. J Contr Rel 2005;104:51–66.

Park JH, Allen MG, Prausnitz MR. Polymer micro-needles for controlled-release drug delivery. Pharm Res 2006;23:1008–19. [PubMed: 16715391]

Park JH, Yoon YK, Choi SO, Prausnitz MR, Allen MG. Tapered conical polymer microneedles fabricated using an integrated lens technique for transdermal drug delivery. IEEE Trans Biomed Eng 2007;54:903–13. [PubMed: 17518288]

Pastorin G, Junginger H, Nayak TR, Munrui Z. Nanoneedles devices for transdermal vaccine delivery: in vitro and in vivo evaluation. Controlled Release Society. July 18–22;2009

Patel SR, Edelhuaser HF, Nickerson JM, Prausnitz MR. Hollow microneedles for suprachoroidal drug delivery to the posterior segment of the eye. Controlled Release Society. July 18–22;2009

Pearton M, Allender C, Brain K, Anstey A, Gateley C, Wilke N, Anthony M, Birchall J. Gene delivery to the epidermal cells of human skin explants using microfabricated microneedles and hydrogel formulations. Pharm Res 2007;25:407–16. [PubMed: 17671832]

Perennes F, Marmiroli B, Matteucci M, Tormen M, Vaccari L, Fabrizio ED. Sharp beveled tip hollow microneedle arrays fabricated by LIGA and 3D soft lithography with polyvinyl alcohol. J Micromech Microeng 2006;16:473–9.

Prausnitz MR. Microneedles for transdermal drug delivery. Adv Drug Deliv Rev 2004;56:581–7. [PubMed: 15019747]

Qiu Y, Gao Y, Hu K, Li F. Enhancement of skin permeation of docetaxel: a novel approach combining microneedle and elastic liposomes. J Contr Rel 2008;129:144–50.

Ramasubramanian MK, Barham OM, Swaminathan V. Mechanics of a mosquito bite with applications to microneedle design. Bioinspir Biomim 2008;3:046001. [PubMed: 18779629] Rodriguez A, Molinero D, Valera E, Trifonov T, Marsal LF, Pallares J, Alcubilla R. Fabrication of silicon oxide microneedles from macroporous silicon. Sens Actuators B 2005;109:135–40.

Roxhed N, Patrick G, Stemme G. Membrane-sealed hollow microneedles and related administration schemes for transdermal drug delivery. Biomed Microdevices 2008a;10:271–9. [PubMed: 17940907]

Roxhed N, Samel B, Nordquist L, Griss P, Stemme G. Painless drug delivery through microneedle-based transdermal patches featuring active infusion. IEEE Trans Biomed Eng 2008b;55:1063–1071. [PubMed: 18334398]

Runyan, WR.; Bean, KE. Silicon Materials Technology. In: Runyan, WR.; Bean, KE., editors. Semiconductor integrated circuit processing technology. Addison-Wesley; New York: 1990. p. 45-56.

Sammoura F, Kang JJ, Heo YM, Tae SJ, Liwei L. Polymeric microneedle fabrication using a microinjection molding technique. Microsyst Technol 2007;13:517–22.

Shikida M, Hasada T, Sato K. Fabrication of a hollow needle structure by dicing wet etching and metal deposition. J Micromech Microeng 2006;16:2230–9.

Shikida M, Sato K, Tokoro K, Uchikawa D. Differences in anisotropic etching properties of KOH and TMAH solutions. Sens Actuators A Physical 2000;80:179–88.

Sivamani RK, Liepmann D, Maibach HI. Microneedles and transdermal applications. Expert Opinion Drug Deliv 2007;4:19–25.

Sivamani RK, Stoeber B, Wu GC, Zhai H, Liepmann D, Maibach H. Clinical microneedle injection of methyl nicotinate: stratum corneum penetration. Skin Res Technol 2005;11:152–6. [PubMed: 15807814]

Stoeber B, Liepmann D. Arrays of hollow out-of-plane micro-needles for drug delivery. J Microelectromech Syst 2005;14:472–9.

Sullivan SP, Murthy N, Prausnitz MR. Minimally invasive protein delivery with rapidly dissolving polymer microneedles. Adv Mater 2008;20:933–938.

Tao SL, Desai TA. Microfabricated drug delivery systems: from particles to pores. Adv Drug Deliv Rev 2003;55:315–28. [PubMed: 12628319]

Teo AL, Shearwood C, Ng KC, Lu J, Moochhala S. Transdermal microneedles for drug delivery applications. Mater Sci Eng 2006;132:151–4.

Thakur RRS, Garland MJ, Cassidy CM, Migalska K, Demir YK, Abdelghany S, Ryan E, Woolfson AD, Donnelly RF. Microporation techniques for enhanced delivery of therapeutic agents. Recent Patents Drug Deliv Formul 2010;4:1–17.

Trichur R, Kim S, Zhu X, Suk JW, Hong C-C, Choi J-W, Ahn CH. Development of plastic microneedles for transdermal interfacing using injection molding techniques. Micro Total Anal Syst 2002;1:395–7.

Trimmer, W.; Ling, P.; Chin, CK.; Orten, P.; Gaugler, R.; Hashmi, S.; Hashmi, G.; Brunett, B.; Reed, M. Injection of DNA into plant and animal tissues with micromechanical piercing structures; Proceedings of the IEEE Microelectromechanical Systems Workshop 8th; Amsterdam. 1995. p. 111-5.

Vemulapalli V, Yang Y, Friden PM, Banga AK. Synergistic effect of iontophoresis and soluble microneedles for transdermal delivery of methotrexate. J Pharm Pharmcol 2008;60:27–33.

Verbaan FJ, Bal SM, Van den DJB, Dijksman JA, Van Hecke M, Verpoorten H, Van den AB, Luttge R, Bouwstra JA. Improved piercing of microneedle arrays in dermatomed human skin by an impact insertion method. J Contr Rel 2008;128:80–8.

Verbaan FJ, Bal SM, van den DJB, Groenink WHH, Verpoorten H, Lüttge R, Bouwstra JA. Assembled microneedle arrays enhance the transport of compounds varying over a large range of molecular weight across human dermatomed skin. J Contr Rel 2007;117:238–45.

Wang PM, Megan C, Hill J, Prausnitz MR. Precise microinjection into skin using hollow microneedles. J Invest Dermatol 2006;126:1080–7. [PubMed: 16484988]

Wang J, Lu J, Suw YL, Maika V, Baomin T, Adeniyi WK, Armendariz RA. Lab-on-a-cable for electrochemical monitoring of phenolic contaminants. Anal Chem 2000;72:2659–63. [PubMed: 10857651]

Wermeling DP, Banks SL, Hudson DA, Gill HS, Gupta J, Prausnitz MR, Stinchcomb AL. Microneedles permit transdermal delivery of a skin-impermeant medication to humans. PNAS 2008;105:2058–63. [PubMed: 18250310]

Widera G, Johnson J, Kim L, Libiran L, Nyam K, Daddona PE, Cormier M. Effect of delivery parameters on immunization to ovalbumin following intracutaneous administration by a coated microneedle array patch system. Vaccine 2006;24:1653–64. [PubMed: 16246466]

Wilke N, Mulcahy A, Ye SR, Morrissey A. Process optimization and characterization of silicon microneedles fabricated by wet etch technology. Microelec J 2005;36:650–6.

Wu XM, Todo H, Sugibayashi K. Enhancement of skin permeation of high molecular compounds by a combination of microneedle pretreatment and iontophoresis. J Contr Rel 2007;118:189–95.

Xie Y, Xu B, Gao Y. Controlled transdermal delivery of model drug compounds by MEMS microneedle array. Nanomed Nanotechnol Biol Med 2005;1:184–90.

Yang M, Zahn JD. Microneedle insertion force reduction using vibratory actuation. Biomed Microdevices 2004;6:177–82. [PubMed: 15377826]

Zafar SR, Thwar PK, Yang M, Ugaz VM, Burns MA. Integrated microsystems for controlled drug delivery. Adv Drug Deliv Rev 2004;56:185–9. [PubMed: 14741115]

Ziaie B, Baldi A, Lei M, Gu Y, Siegel RA. Hard and soft micromachining for BioMEMS: review of techniques and examples of applications in microfluidics and drug delivery. Adv Drug Deliv Rev 2004;56:145–8. [PubMed: 14741113]

Zosanopharma. Zosano's Macroflux. Available online at: http://www.zosanopharma.com/, accessed 1 October 2009

UKPMC Funders Group Author Manuscript

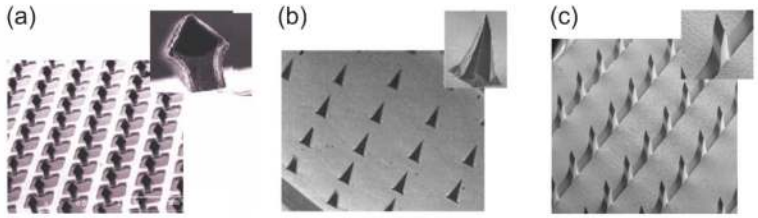

Figure 1.
Scanning electron microscope (SEM) images of (a) in-plane MNs (Daddona, 2002), (b) out-of-plane MNs (Donnelly et al., 2009b), and (c) combined in-plane and out-of-plane MNs (Jae-Ho et al., 2008).

UKPMC Funders Group Author Manuscript

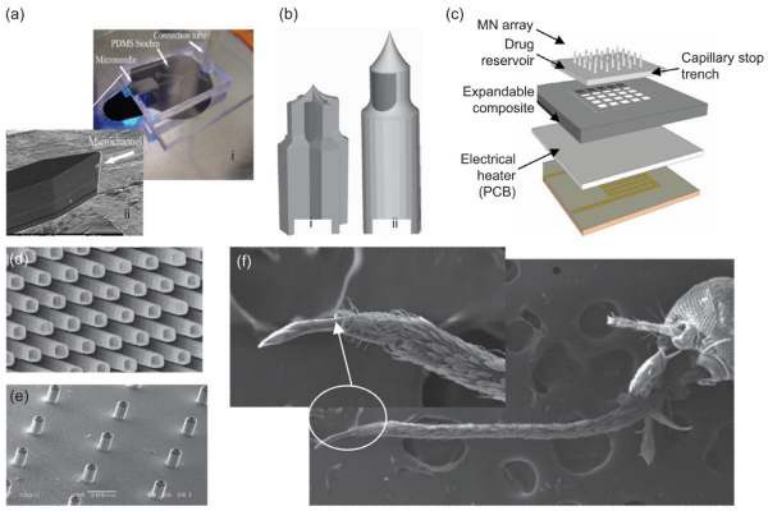

Figure 2.

SEM micrographs of variety of a hollow silicon MNs: (a) (i) PDMS microfluid chip integrated MN array with a (ii) microchannel entrance at the tip (Paik et al., 2004). (b) Cross- and circular-shaped HMNs with side-opening (Roxhed et al., 2008a). (c) Patch-like MN integrated dispensing unit (Roxhed et al., 2008b). (d) Array of MNs with 70 nm wall thickness and square arrangement (Rodriguez et al., 2005). (e) MN array integrated to a PZT pump (Bin et al., 2006). (f) Mosquito head and proboscis, the inset shows the magnified view of fascicle tip with labella retracted (Ramasubramanian et al., 2008).

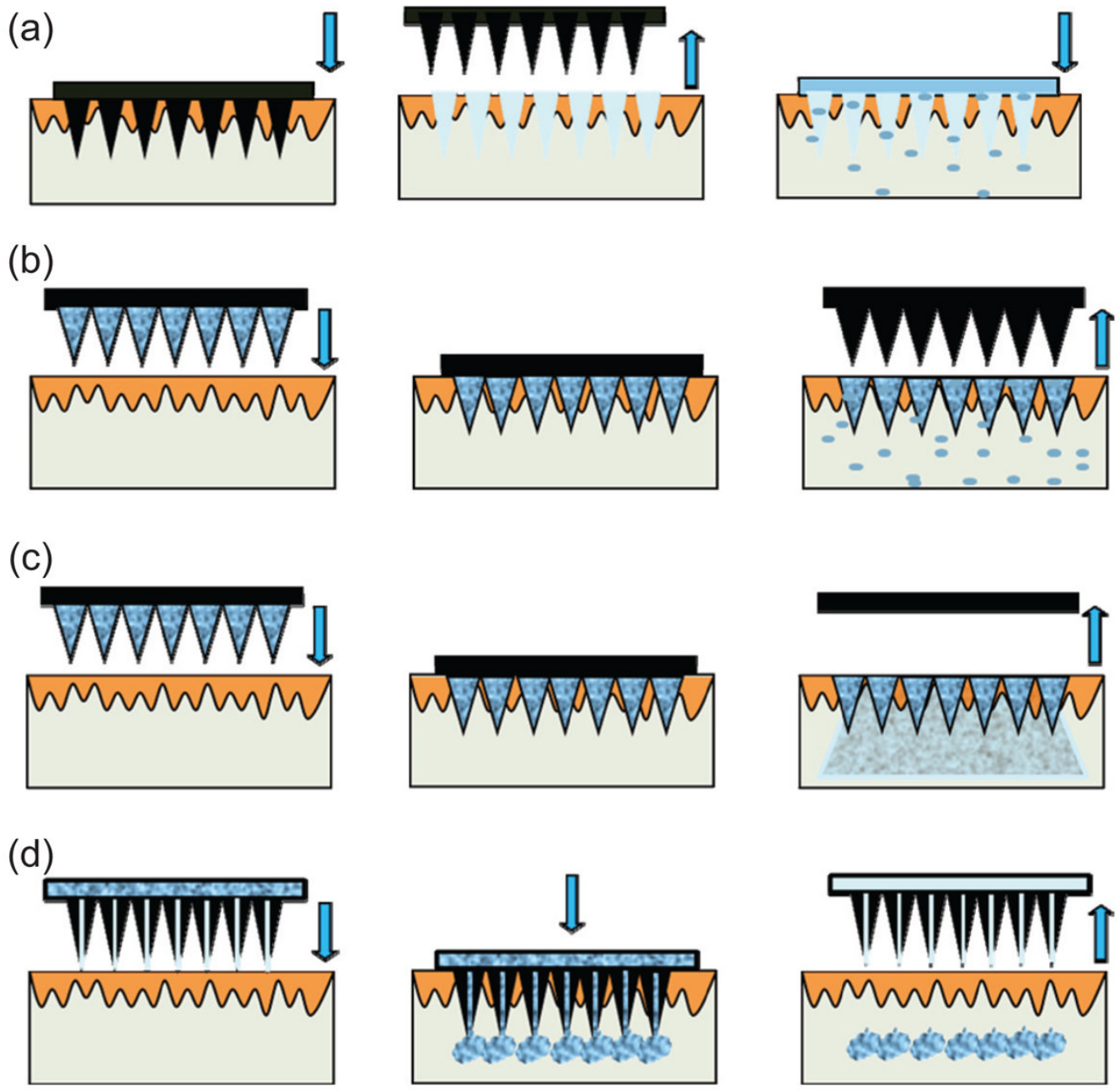

Figure 3.
Schematic representation of different methods of MN application across the skin. (a) Solid MNs applied and removed to create micropores followed by the application of a traditional transdermal patch. (b) Solid MNs coated with drug molecules applied for instant delivery. (c) Polymeric MNs which remain in skin and dissolve over time to deliver the drug within the MNs. (d) Hollow MNs for continuous drug delivery or body fluid sampling. Adapted from Arora et al. (2008).

UKPMC Funders Group Author Manuscript

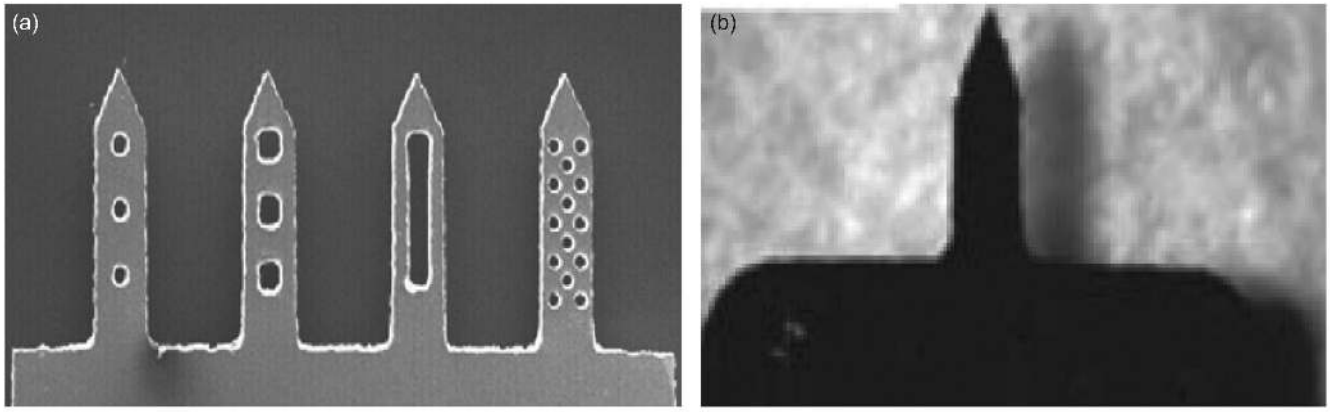

Figure 4.
Images of (a) MNs with ‘pockets’ of different shapes and sizes etched through the MN shaft (Gill & Prausnitz, 2007a). (b) Brightfield microscopy image of a single solid stainless-steel MN (Gill & Prausnitz, 2008).

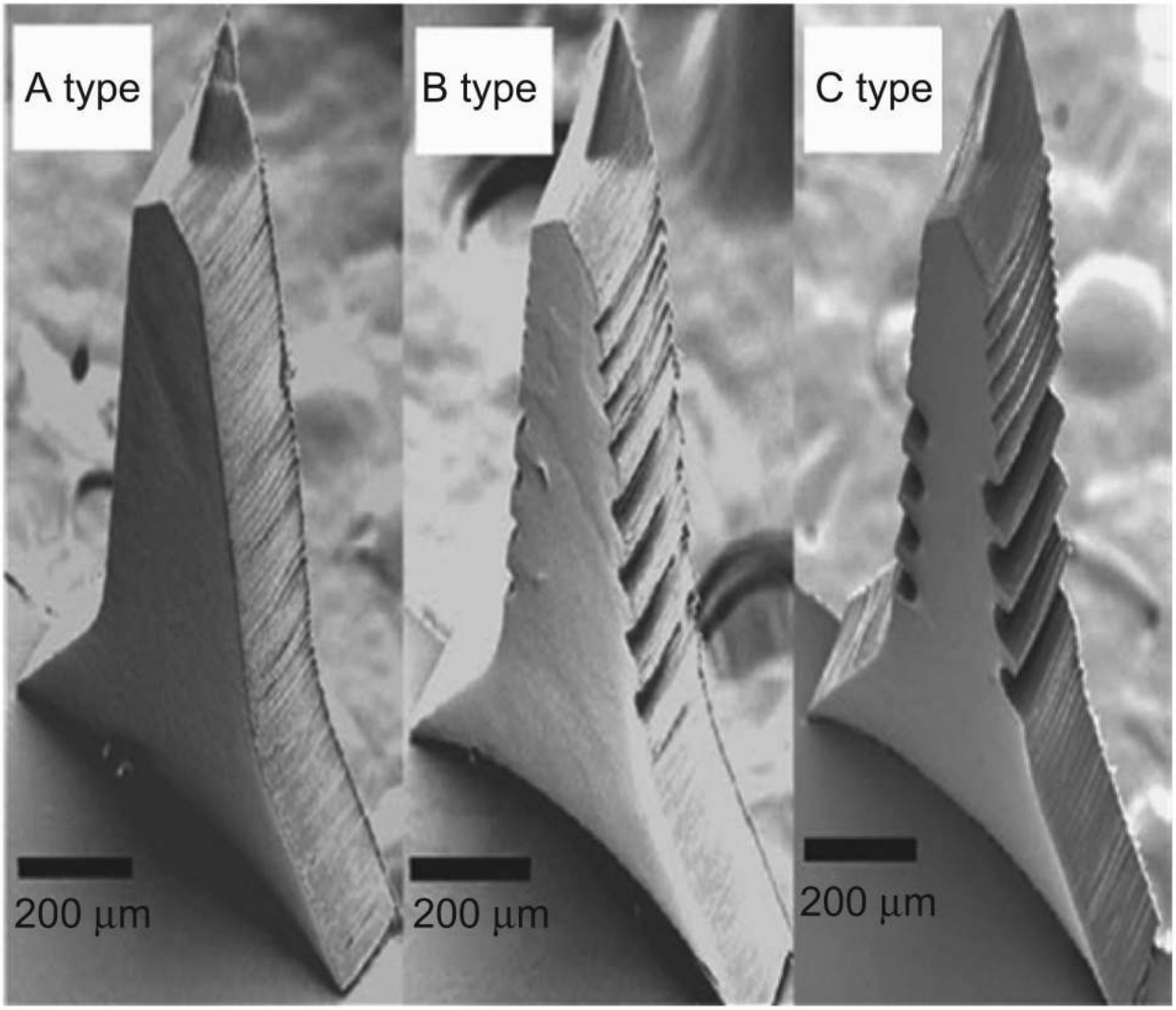

Figure 5.
SEM images of groove-embedded MNs (Han et al., 2009).

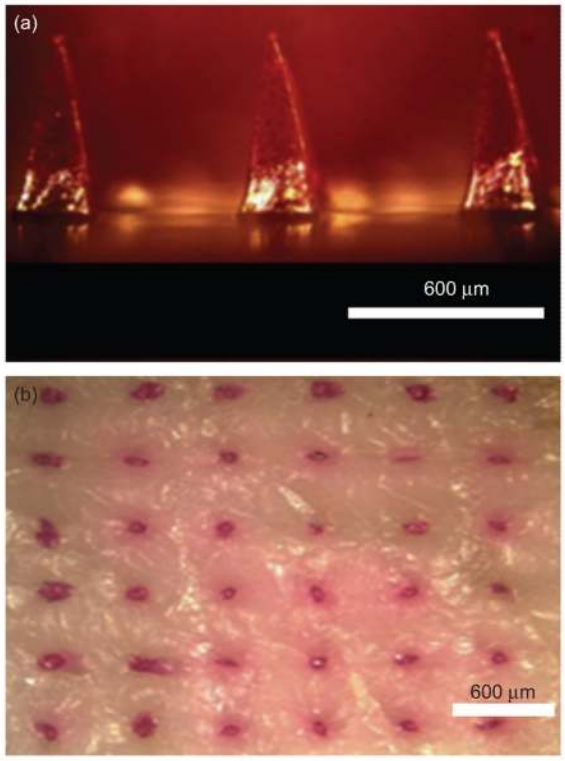

Figure 6.
Dissolving MNs for transdermal drug delivery. (a) CMC pyramidal MNs encapsulating sulforhodamine B within the MN shafts, but not in the backing layer. (b) Skin surface showing MN delivered sulforhodamine B.

UKPMC Funders Group Author Manuscript

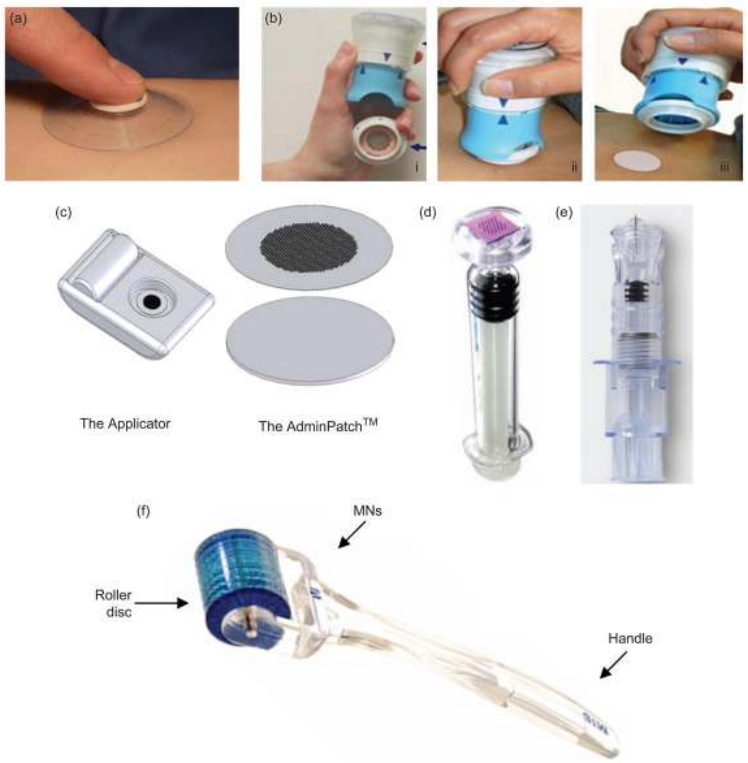

Figure 7.
MN applicators from different companies. (a) MicroCor™ applicator. Adapted from Gary (2009). (b) Zosano's Macroflux® (i) applicator loaded with patch, (ii) applicator activated, (iii) patch delivered to the site. Adapted from Zosanopharma® (2009). (c) AdminPatch® MN array applicator. Adapted from Nanobiosciences® (2009). (d) MicronJet® MN device. Adapted from Nanopass® (2009). (e) BD Soluvia™ applicator. Adapted from BD (2009). (f) MTS-Rollers™ applicator. Adapted from Microneedle® (2009).